(2)

NAVAL POSTGRADUATE SCHOOL

Monterey, California

THESIS

CLOUD EFFECTS ON OCEAN MIXED LAYER
IN THE NORTHEAST PACIFIC OCEAN

by

Pao-Kun Wu

June 1991

Thesis Advisor: Pecheng Chu
Co-Advisor: Roland W. Garwood

Unclassified

Security Classification of this page

REPORT DOCUMENTATION PAGE

1a Report Security Classification UNCLASSIFIED	1b Restrictive Markings
2a Security Classification Authority	3 Distribution Availability of Report: Approved for public release; distribution is unlimited.
2b Declassification/Downgrading Schedule	
4 Performing Organization Report Number(s)	5 Monitoring Organization Report Number(s)
6a Name of Performing Organization: Naval Postgraduate School; 6b Office Symbol (*If Applicable*): 68Cu	7a Name of Monitoring Organization: Naval Postgraduate School
6c Address (*city, state, and ZIP code*): Monterey, CA 93943-5000	7b Address (*city, state, and ZIP code*): Monterey, CA 93943-5000
8a Name of Funding/Sponsoring Organization; 8b Office Symbol (*If Applicable*)	9 Procurement Instrument Identification Number
8c Address (*city, state, and ZIP code*)	10 Source of Funding Numbers: Program Element Number; Project No; Task No; Work Unit Accession No

11 Title (*Include Security Classification*) CLOUD EFFECTS ON OCEAN MIXED LAYER IN THE NORTHEAST PACIFIC OCEAN

12 Personal Author(s) PAO-KUN WU

13a Type of Report	13b Time Covered	14 Date of Report (*year, month,day*)	15 Page Count
Master's Thesis	From To	1991, June	79

16 Supplementary Notation The views expressed in this paper are those of the author and do not reflect the official policy or position of the Department of Defense or the U.S. Government.

17 Cosati Codes			18 Subject Terms (*continue on reverse if necessary and identify by block number*)
Field	Group	Subgroup	Air-sea interaction; Northeast Pacific Ocean

19 Abstract (*continue on reverse if necessary and identify by block number*

This study was conducted to examine the effect of clouds on the ocean mixed layer, both short-term and seasonal. It utilized data collected at Ocean Station Papa in the northeast Pacific. Two numerical modeling simulations were performed (i.e. with variable cloud and with variable precipitation). The results of the variable cloud simulation indicated that the downward surface buoyancy flux and longer daylight period in summer may induce a significant albedo effect of cloud on ocean mixed layer. The upward surface buoyancy flux and longer night period in winter will result in a pronounced greenhouse effect of cloud on ocean mixed layer. The results of variable precipitation simulation showed that the mixed layer is most sensitive to precipitation between October and March.

Model predictions are verified using data at Ocean Station Papa for monthly and yearly mean values of cloud cover and precipitation. The comparison between model prediction and observations shows that the mean values of observed MLD ($\overline{H} = 60.9m$) are much deeper than model-predicted values ($\overline{H} = 36.5m$).

20 Distribution/Availability of Abstract	21 Abstract Security Classification	
[X] unclassified/unlimited [ ] same as report [ ] DTIC users	Unclassified	
22a Name of Responsible Individual: P. Chu	22b Telephone (*Include Area code*): (408) 646-2768	22c Office Symbol: 68Cu

DD FORM 1473, 84 MAR 83 APR edition may be used until exhausted

All other editions are obsolete

security classification of this page

Unclassified

Approved for public release; distribution is unlimited

CLOUD EFFECTS ON OCEAN MIXED LAYER IN THE NORTHEAST PACIFIC OCEAN

by

Pao-Kun Wu
Lieutenant Commander, Chinese Navy
B.S., Chinese Naval Academy, 1979

Submitted in partial fulfillment of the
requirements for the degree of

MASTER OF SCIENCE IN PHYSICAL OCEANOGRAPHY

From the

NAVAL POSTGRADUATE SCHOOL
June 1991

Author: Wu Pao Kun
Pao-Kun Wu

Approved by: Pecheng Chu
Pecheng Chu, Thesis Advisor

Roland W. Garwood, Co-Advisor

Curtis A. Collins
Curtis A. Collins, Chairman
Department of Oceanography

ABSTRACT

This study was conducted to examine the effects of clouds on the ocean mixed layer, both short-term and seasonal. It utilized data collected at Ocean Station Papa in the northeast Pacific. Two numerical modeling simulations were performed (i.e. with variable cloud and with variable precipitation). The results for the variable cloud simulation indicated that the downward surface buoyancy flux and longer daylight period in summer may induce a significant albedo effect of cloud on ocean mixed layer. The upward surface buoyancy flux and longer night period in winter will result in a pronounced greenhouse effect of cloud on ocean mixed layer. The results of variable precipitation simulation showed that the mixed layer is most sensitive to precipitation between October and March.

Model predictions are verified using data at Ocean Station Papa for monthly and yearly mean values of cloud cover and precipitation. The comparison between model prediction and observations shows that the mean values of observed MLD ($\overline{H}$ = 60.9 m) are much deeper than model-predicted values ($\overline{H}$ = 36.5 m).

TABLE OF CONTENTS

LIST OF TABLES

LIST OF FIGURES

ACKNOWLEDGEMENT

The author wishes to express sincere gratitude to Dr. Pecheng Chu for his guidance and support throughout the research and preparation of this thesis and to Dr. R. W. Garwood who provided the OPBL model and solutions to many of the problems encountered in the research. Their enthusiasm and confidence in me and in the worthiness of this study were unflagging.

I. INTRODUCTION

In general, both clouds and precipitation can have a significant influence on upper ocean dynamics. Alteration of short wave and long wave radiation at the ocean surface caused by clouds and variation of upper ocean salinity caused by precipitation and evaporation may also change the ocean mixed layer structure. Very few one-dimensional mixed layer experiments had previously explained how the clouds and precipitation affect the ocean mixed layer. It might be that the cloud amount and precipitation were inaccurately observed or measured, or that the water mass flux has been given less attention by oceanographers, although it is realized that clouds and precipitation contribute to the surface buoyancy flux that influences depth and temperature in the ocean mixed layer.

It is the intention of this study to examine the effects of clouds on the evolution of the gross thermodynamic properties of the ocean mixed layer. Employing data derived from observations taken at Ocean Station Papa (50°N, 145°W) we shall focus specifically on the short and long-term fluctuating relationship between degree of cloud cover and its oceanic consequences.

Earlier studies of ocean mixed layer dynamics dealt explicitly with equations for the production, alteration and destruction of turbulent kinetic energy within the mixed layer. Kraus and Turner (1967) were the first to examine the turbulent kinetic energy budget in a one-dimensional mixed layer model for the ocean, using the approximately decoupled equations for the thermal and mechanical energy. It was assumed that the heat input at the ocean surface was known, and the water mass entrainment at the base of the

mixed layer needed to be predicted. The wind stress is treated as a production term that generates the turbulent kinetic energy for mixing. The entrainment was associated with wind energy input to the water column minus the work performed in overcoming the buoyancy flux throughout the mixed layer. The problem of the Kraus-Turner model was that it only considered the heat flux and wind forcing and neglected the viscous dissipation and salinity effects. The dissipation was assumed to be a fixed fraction of wind stress production in the model of Geisler and Kraus (1969), Miropol'skiy (1970) and Denman (1973). The further parameterization of dissipation is needed in certain instances (Elsberry et al. (1976), and Kim (1976)).

The first study which considered salinity and its effects on the density structure in the ocean mixed layer was by Miller (1976). In his study, he indicated that without salinity effect, the cooling induced by entrainment was greater than the heating from the surface, resulting in ocean mixed layer cooling. On the other hand, with salinity included the layer deepens more slowly and entrains less cold water at the bottom allowing surface heating to dominate which causes the mixed layer temperature to increase.

A one-dimensional bulk model of ocean mixed layer which included dynamic instability with turbulent erosion was introduced by Garwood (1977). This model modulates the mean entrainment rate by diurnal heating and limits maximum layer depth by enhancing the effect of viscous dissipation. His study also included the possibly important effect of long-term salinity fluxes on the mixed layer thermal profile due to surface heat fluxes, precipitation and entrainment at the base of the mixed layer. This model was chosen for this study.

Livezey(1988) used an oceanic mixed layer model to examine the effects of discrete precipitation events on the short-term and seasonal evolution of ocean mixed layer temperature and salinity structure at Ocean Station Papa. He indicated that the effect of precipitation on ocean mixed layer largely depends on the strength of wind forcing. When wind speed is low, the fluctuation of mixed layer temperature and salinity will be considerably enhanced by the precipitatioin. The model results suggest that the amount of precipitation observed at Ocean Station Papa was too low to explain the observed ocean salinity structure for the year.

The importance of cloud cover on the mid-latitude ocean mixed layer has not been investigated in a numerical model, although it plays an important role in heat budget of the ocean surface. Recent work about the thermodynamical process between cloud and tropical ocean mixed layer was introduced by Chu and Garwood (1989, 1990). They show that the ocean mixed layer and clouds are coupled by both heat and moisture fluxes across the air-ocean interface. In this coupled system, as far as the turbulent kinetic energy is concerned, the fresh water influx at the ocean surface due to excess precipitation over evaporation is a damping factor and the surface cooling caused by reduction of solar radiation at the ocean surface by cloud is a forcing factor. The aim of this study is to examine the effects of these two factors on the mid-latitude ocean mixed layer dynamic by using meterological and oceanographic observations in 1959 at Ocean Station Papa.

II. EFFECT OF CLOUD ON OCEAN MIXED LAYER

Generally speaking, there exist two thermodynamic processes in the coupled cloud-ocean mixed layer system. First, the incoming solar radiation at the ocean surface will be reduced by scattering and absorption of cloud, which cools the ocean surface layer and increases mixed layer entrainment. This is a forcing factor. Second, if rainfall begins, the precipitation will dilute the surface salinity, stabilizing the upper layer and decreasing mixed layer entrainment. This is a damping factor. Figure 1 shows the relation between the clouds and ocean mixed layer (Chu and Garwood 1989).

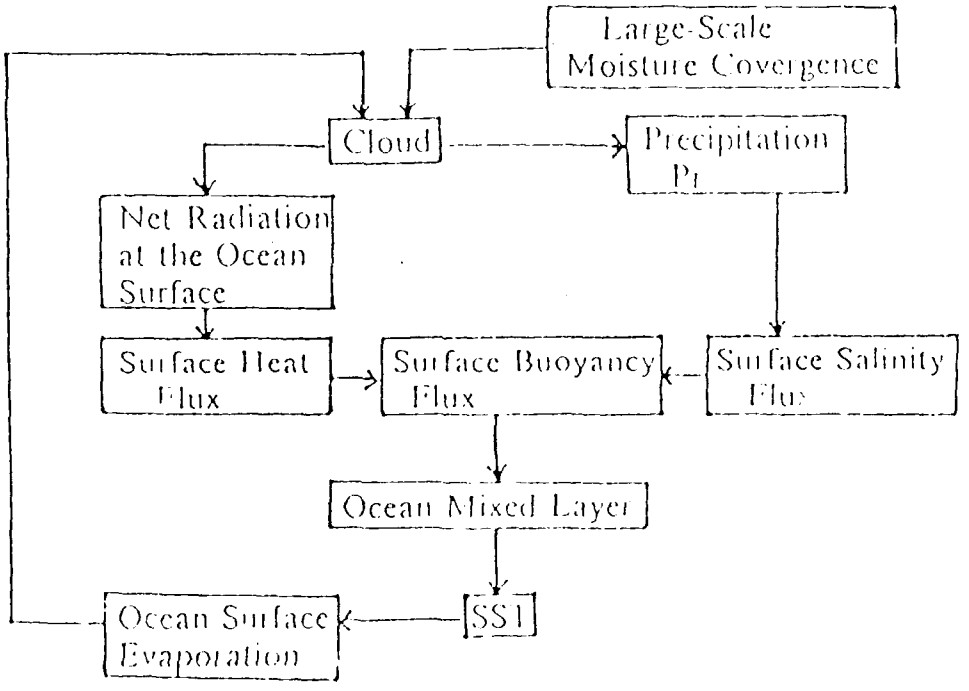

Figure 1. The Relationship between Clouds and Ocean Mixed Layer

It should be mentioned that deepening or shallowing of the ocean mixed layer depends on the ocean surface buoyancy flux and surface wind stress. Wind stress always generates turbulence, tending to deepen the mixed layer. However, the buoyancy flux has two different effects. Upward buoyancy flux make the water column statically unstable, which generates turbulence and deepens the ocean mixed layer. Downward buoyancy flux makes the water column statically stable, which damps the turbulence and possibly shallows the ocean mixed layer. When the ocean mixed layer deepens, the mixed layer entrains water from below and increases the potential energy. If there is relatively stronger downward buoyancy flux, the shear production may be insufficient to overcome the buoyant damping and turbulence cannot reach the former mixed layer depth, causing mixed layer retreat.

In the diurnal period, the clouds also have two important effects on the radiation balance at the ocean surface: namely, an albedo effect when the downwelling solar radiation is decreased due to reflection and absorption of incoming solar radiation by clouds during the daytime, and a greenhouse effect when the upwelling longwave radiation is decreased due to the emission of long wave radiation back to the ocean's surface by clouds. The albedo effect on ocean mixed layer is dependent on diurnal and seasonal variations of solar radiation. During summer, solar radiation is stronger, therefore the albedo effect of cloud significantly impact the ocean mixed layer. In contrast, the clouds have less influence on ocean mixed layer during the winter season due to the domination of shear production in ocean mixed layer dynamics. The effect of precipitation on ocean mixed layer also has seasonal variation.

Since both long and short-term clouds can be shown to have significant effect on the dynamic changes that occur within the ocean mixed layer, its importance as a central element in any prognostification of the mixed layer cannot be overlooked or underestimated.

III. BACKGROUND DATA

Ocean Station Papa is at the geographic position (50°N, 145°W) where a Canadian weather ship used to be continuously stationed. It is located in the eastern part of the subarctic Pacific region on the southern edge of the Alaska Gyre. The dominant atmospheric pressure systems located in the North Pacific Ocean are the Aleutian Low in winter and the North Pacific High in summer. These two systems control the distribution of surface winds over the Northeast Pacific Ocean. In winter, the Aleutian Low directs air flow northward into the Gulf of Alaska, and in summer the North Pacific High directs winds southeast at Ocean Station Papa. The direction of the monthly winds does not significantly change from season to season, but the magnitudes of the winds are about twice as high in winter (13 m/s) as in summer (6 m/s). Because of the large-scale influence of the wind systems over the North Pacific Ocean, the surface waters flow eastward across the North Pacific. Ocean Station Papa lies in the path of this flow as shown in Figure 2.

According to Thompson (1971), typical geostrophic currents are in an east-northeast direction, roughly parallel to surface isotherms and isopycnals, with a speed around 1 cm/s. Wind induced surface drift currents and inertial currents may be as large 50 cm/s, but since they are typically either transient or oscillatory they do not contribute appreciably to advection on a longer time scale.

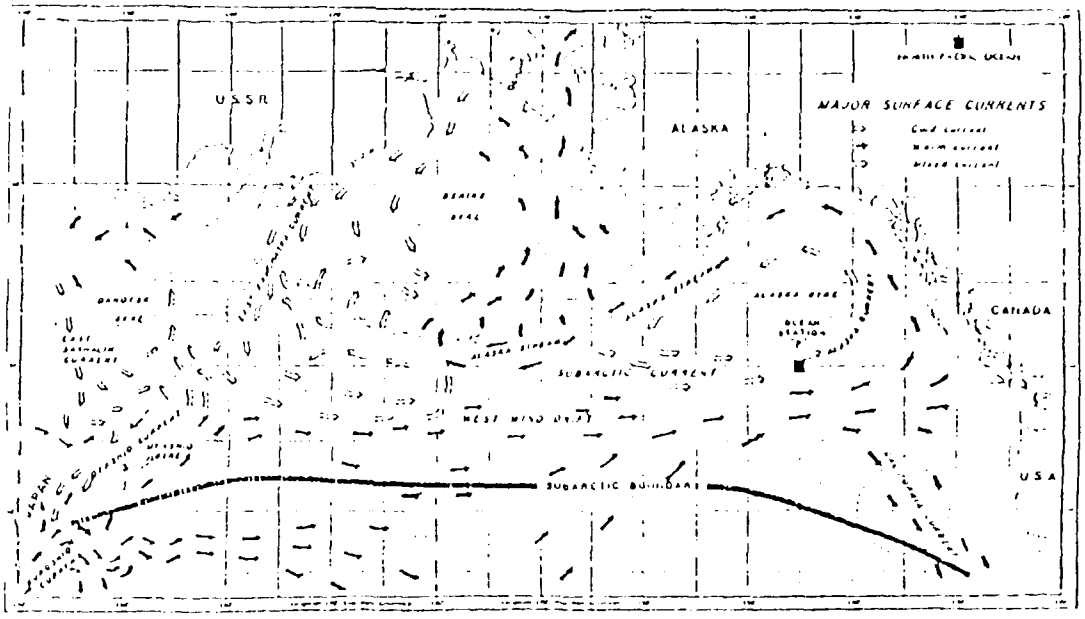

Figure 2. Major Surface Ocean Currents in the Sub-Arctic Region (adapted from Uda, 1963)

The influence of horizontal advection at Ocean Station Papa can be estimated from horizontal currents and temperature gradient. For a typical surface temperature gradient in the northeast Pacific of about 1°C $(100\ km)^{-1}$ and currents of 1– 10 km day^{-1}, the maximum temperature change to be expected from advective effects would be about 1°C in 10 days (Denman and Miyake, 1973). Tabata (1965) attempted to estimate the temperature and salinity change at Papa attributable to horizontal advection. He concluded that the average monthly temperature change at Papa due to advective effects for a five-year period was 0.26°C $month^{-1}$, with a maximum of 0.78°C $month^{-1}$. The average monthly salinity change was 0.02 ppt $month^{-1}$, with a maximum of 0.05 ppt $month^{-1}$. During the warming season, change in sea surface temperature associated with synoptic-scale weather patterns are of the

order of 1°C over several days (Denman and Miyate, 1973). Tabata (1961, 1965) and Thomson (1971) examined the vertical structure of the ocean at Papa in some detail. At Papa the main or permanent pycrocline occurs between 100 and 200 m, where the salinity increases from 32.8 ppt to 33.8 ppt, the temperature decreases from 4.5 to 4.0°C, and consequently, σ_t increases from 26.0 to 26.8. In summer, the seasonal thermocline forms in the upper 75m, where the temperature variation dominates the density variation. During winter season, the salinity variations associated with the large evaporation at the sea surface may become significant.

Tabata (1961) indicated that there is an annual average excess of precipitation over evaporation of 0.5m in the vicinity of Ocean Station Papa. At Ocean Station Papa, the monthly mean precipitation(P_r), evaporation(E), and E–P_r are shown in Figure 3. The cloud cover variation (about 1/2 during winter and 1 during summer) is shown in Figure 4. These two data sets are the input data used to drive the NPS mixed layer model.

There are three reasons for using this data set for this study: (1) cloudy days occurring frequently in the vicinity of Ocean Station Papa, (2) salinity varies significantly in the winter season, and (3) there are about 30 years of continuous meteorological and oceanographic data in this region.

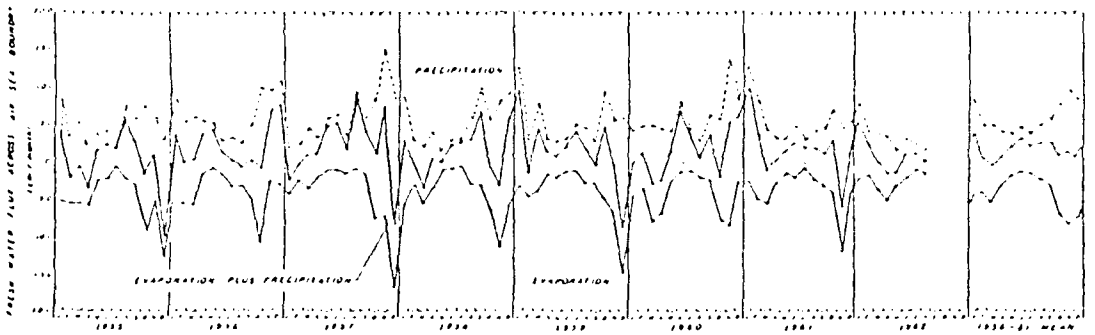

Figure 3. Monthly Mean Values of Precipitation, Calculated Evaporation, and $E - P_r$ at Ocean Station Papa (from Tabata, 1965)

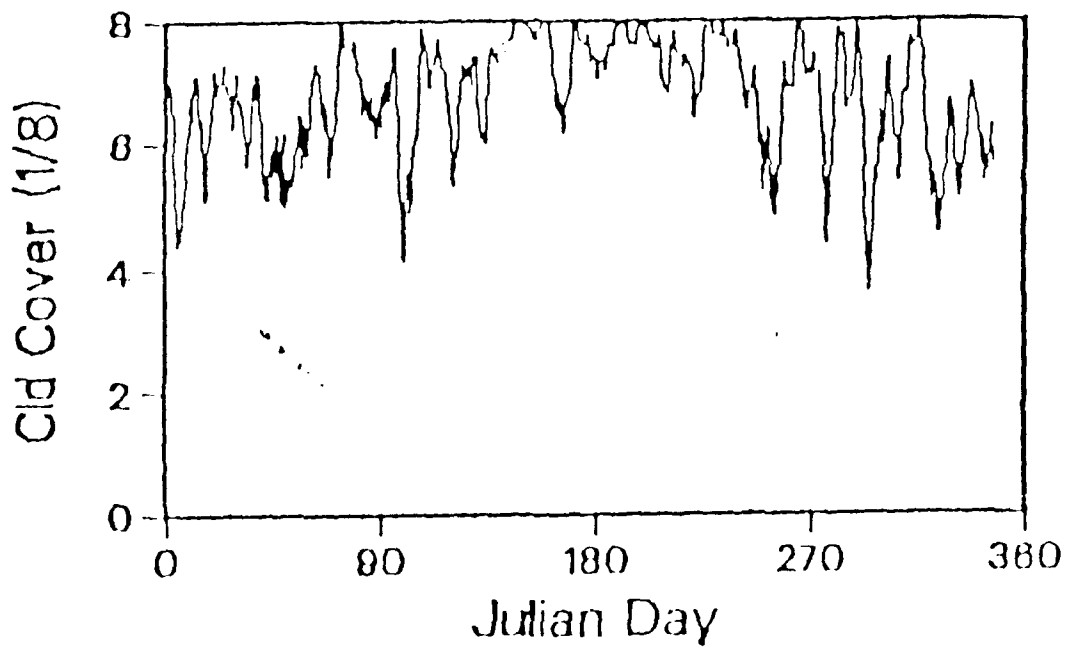

Figure 4. Cloud Cover Variation at Ocean Station Papa in 1959 (from Garwood and Adamec, 1982)

IV. BASIC THEORY OF THE NPS MIXED LAYER MODEL

A. OCEAN MIXED LAYER STRUCTURE

The upper layer of the ocean is a region in which the water temperature is nearly isothermal. In the Oceanic Planetary Boundary Layer (OPBL), mixing due to wind stirring and upward buoyancy flux maintains the nearly homogeneous temperature and salinity profile. Depending on the strength of the winds and on the direction of the surface heat flux, the depth of the mixed layer can be as shallow as a few centimeters or as deep as two hundred meters or more. Figure 5 shows an idealized temperature profile of the upper ocean. An isothermal layer of temperature T exists in the uppermost h meters. Below this, there is typically a positive temperature jump ΔT, over a small vertical distance Δh. Below $z = -h - \Delta h$, the temperature decreases with increasing depth.

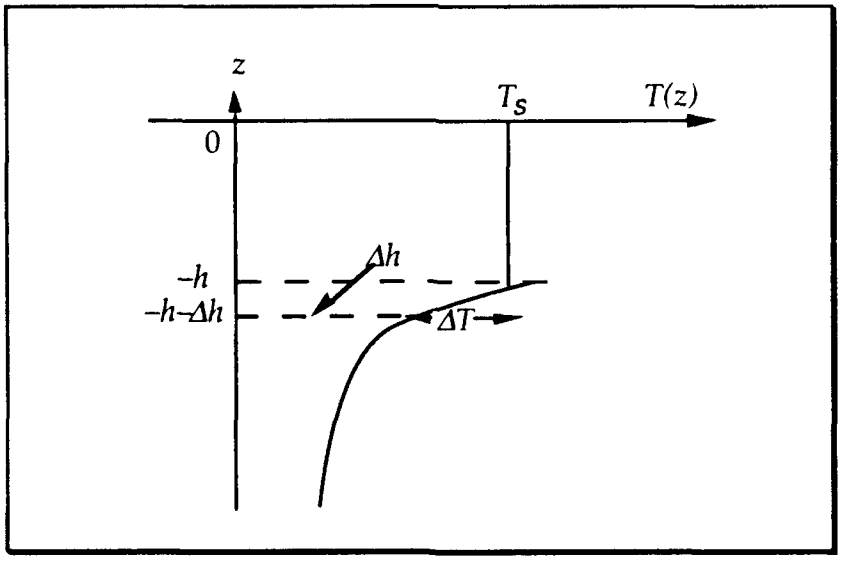

Figure 5. Idealized Temperature Profile for Upper 200 m of the Ocean

The characteristics of salinity within the mixed layer structure are similar to those of temperature (Figure 6). There is a relatively constant salinity from $z = 0$ to $z = -h$. A corresponding jump in salinity then occurs across the entrainment zone from $z = -h$ to $z = -h-\Delta h$, followed by gradually increasing increments of salinity within the depths below the mixed layer. The sign of ΔS may be positive or negative, depending upon the history of net precipitation minus evaporation, P_r-E.

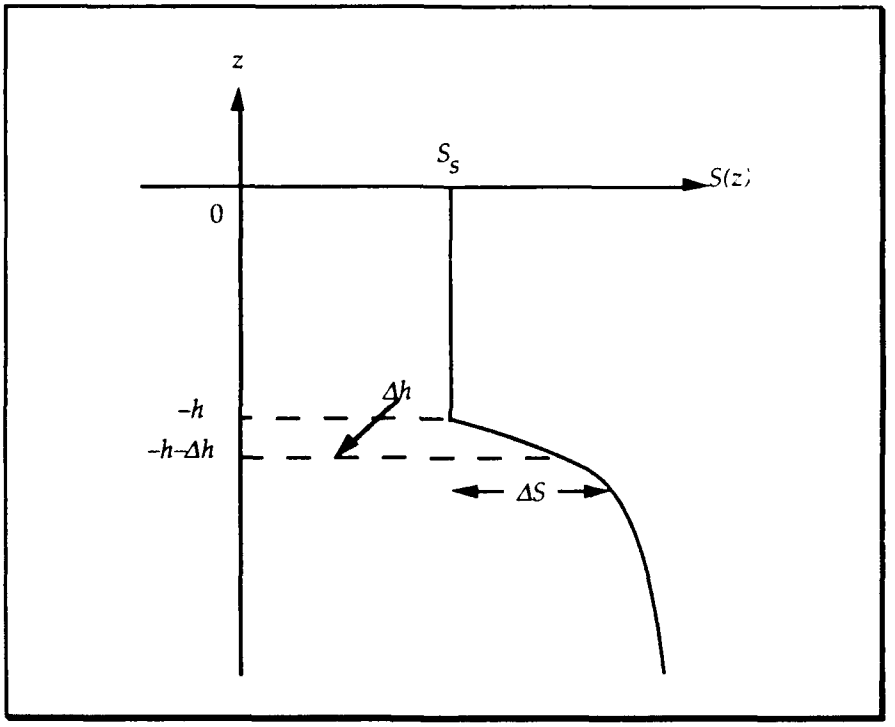

Figure 6. Idealized Salinity Profile for the Upper 200 m of the Ocean

B. THE BASIC EQUATIONS OF THE NPS MIXED LAYER MODEL

For most one-dimensional ocean mixed layer theories, the vertical mixing within the turbulent boundary layer and entrainment mixing at its base occur in response to local atmospheric forces—the surface wind stress

and the buoyancy flux at the sea surface. The buoyancy flux is attributable to net heat flux (including radiation), evaporation and precipitation. The shear production of turbulence is attributable to surface wind stress. The mixed layer temperature T_s, salinity S_s, and depth h are predicted by a simplified form of the NPS mixed layer model (Garwood,1977) modified to include salinity and advection:

$$h\frac{\partial T_s}{\partial t} = -w_e(T_s - T_{-h}) - \frac{Q_0}{\rho_w C_p} \tag{2.1}$$

$$h\frac{\partial S_s}{\partial t} = -w_e\,(S_s - S_{-h}) + (E - P_r)S_s \tag{2.2}$$

Here h is the mixed layer depth, C_p is specific heat for sea water under constant pressure, ρ_w is the characteristic water density, E is the surface evaporation, Pr is the precipitation, and w_e is the entrainment velocity parameterized as:

$$w_e = \frac{|w'|\langle \overline{E} \rangle}{hg[\alpha\Delta T - \beta\Delta s]} \tag{2.3}$$

where $\Delta T = T_s - T_{-h}$ and $\Delta S = S_s - S_{-h}$.

To solve equation (2.3) for w_e, the value of $\langle \overline{E} \rangle$, $|w'|$, T, h and ΔT must be known, together with constant g and α. From Garwood (1977) the total turbulent kinetic energy (TKE) is solved by using:

$$\frac{\partial}{\partial t}\left(h\langle \overline{E} \rangle\right) = G_0 + G_h - B_0 - B_h - D. \tag{2.4}$$

where

$$G_0 = 12\left[\left(\frac{\tau_x}{\rho}\right)^2 + \left(\frac{\tau_y}{\rho}\right)^2\right]^{\frac{3}{4}} \tag{2.5}$$

is the wind stress production,

$$G_h = \left[\langle \overline{u} \rangle^2 + \langle \overline{v} \rangle^2\right] w_e \tag{2.6}$$

is the entrainment shear production,

$$B_0 = \alpha g\left(Q_0/\rho_\omega c_p\right) - \beta g S_s (E - P_r) \tag{2.7}$$

is the buoyant damping or production due to surface buoyancy flux,

$$B_h = \alpha g h \Delta T w_e \tag{2.8}$$

is the buoyant damping due to entrainment, and

$$D = 2\langle \overline{E} \rangle^{\frac{3}{2}} \tag{2.9}$$

is dissipation.

The time rate of change in mixed layer depth is computed by

$$\frac{\partial h}{\partial t} = w_e - w_{-h} \tag{2.10}$$

where w_{-h} is the upwelling velocity specified at the bottom of the mixed layer.

C. CLOUD EFFECT ON HEAT FLUX AT THE OCEAN SURFACE

There are two important effects of clouds on the buoyancy flux (B_0) at the ocean surface: (1) decrease in downward buoyancy flux by reducing the incoming solar radiation or (2) decrease in upward buoyancy flux by emitting the long wave radiation back to the ocean surface. Additionally, the salinity

flux caused by precipitation also can increase downward buoyancy flux indirectly.

The surface heat flux (upward positive), Q_0, is computed by

$$Q_0 = Q_b - Q_s + L\rho_\omega E + Q_h \tag{2.11}$$

where Q_s is the incoming solar radiation absorbed by the ocean surface, Q_b is the net back radiation, L is the latent heat of vaporization of water, Q_h is the sensible heat flux to the air.

The surface evaporation, E, and sensible heat flux from the ocean surface, Q_h, are estimated using the bulk aerodynamic formulae:

$$E = \rho_a C_D U_{10} C_E \left(q_s(T_s) - q_0\right) / \rho_w \tag{2.12}$$

$$Q_h = \rho_a C_p^{(a)} C_D U_{10} C_H (T_s - T_{a0}) \tag{2.13}$$

where C_D is the drag coefficient, taken as 0.001 in this study, U_{10} is the wind speed at 10 m height, $q_s(T)$ is the saturated mixing ratio, T_{a0} is the air temperature at the ocean surface, $C_p^{(a)}$ is specific heat of the atmosphere, C_H,C_E are heat and moisture transfer coefficients. In this study we assume $C_E = C_H$.

Clouds reduce the solar radiation upon the ocean surface by scattering and absorption which is computed by

$$Q_s = \left(1 - a\alpha^b\right)\left(1 - 1.289 \times 10^{-3} C^3\right) Q_c \tag{2.14}$$

where C is the proportion in eighths of a sky covered by cloud, and Q_c is the clear sky radiation given by (Seckel and Beaudry, 1973)

$$Q_c = A_0 + A_1 \cos\phi + B_1 \sin\phi + A_2 \cos 2\phi + B_2 \sin 2\phi. \tag{2.15}$$

The constant a and b are adopted from Tabata (1964) and the cubic cloud cover correction from Laevastu (1960). Noon altitude of the sun is α. The coefficients (A_0, A_1, A_2, B_1, B_2) were calculated by harmonic representation of the values listed in the Smithsonian Meteorological Table, and

$$\phi = \left(\frac{2\pi}{365}\right)(t-21) \tag{2.16}$$

where t is the Julian day of the year.

The ocean surface emits longwave radiation to the atmosphere. The clouds, as well as dry air, partially absorb the radiation and reemit longwave radiation back to the ocean surface. Thus the net back radiation Q_b, is corrected for the downward radiation by the clouds. The net back radiation is estimated from the empirical formula (Husby and Seckel, 1978)

$$Q_b = 1.14\times10^{-7}(273.16+T_s)^4\left(.39-.5E_a^{1/2}\right)\left(1-9.375\times10^{-3}C^2\right). \tag{2.17}$$

Here, T_s is sea surface temperature, E_a is the vapor pressure of air based on the dew-point temperature.

D. SALINITY EFFECT ON MIXED LAYER DYNAMICS

1. The Shallowing Regime

When the ocean surface is strongly heated or there is heavy precipitation, the mixed layer depth is taken as:

$$h = \frac{C_1}{C_2}\frac{u_*^3}{\alpha g Q_0/\left(\rho_w C_p\right)} = L \tag{2.18}$$

where L is the Obokhov length scale, u_* is the water surface friction velocity, which is computed by $u_*^2 = (\rho_a/\rho_w)C_D U_{10}^2$ If the precipitation and evaporation are included, equation (2.18) becomes

$$h = \frac{C_1}{C_2} \frac{u_*^3}{\alpha g Q_0 / (\rho_\omega C_p) + \beta g (P_r - E) S}. \tag{2.19}$$

The heat equation for the shallowing regime is:

$$\frac{\partial T}{\partial t} = \frac{Q_0}{\rho_w C_p h}. \tag{2.20}$$

As a result, precipitation minus evaporation influences mixed layer temperature indirectly. For downward buoyancy flux, a positive $(P_r - E)$ will decrease h, and concentrate the heat into a shallower layer. For the case where evaporation exceeds precipitation, a decrease of mixed layer temperature would be expected.

2. The Entrainment Regime

For an entraining mixed layer, the buoyancy discontinuity at the bottom of the mixed layer is:

$$\Delta b = \alpha g \Delta T - \beta g \Delta S \tag{2.21}$$

the time rate of change of mixed layer salinity is

$$\frac{\partial S_s}{\partial t} = \frac{S_s (E - P_r)}{h} - \frac{w_e \Delta \bar{S}_s}{h}. \tag{2.22}$$

Equation (2.22) demonstrates that the time rate of change of salinity depends on surface fresh water influx and entrainment processes.

E. METHOD OF SOLUTION

Prediction of the rate of deepening (or retreat) of the NPS mixed layer model depends upon an understanding of the dynamics of the entrainment process. The turbulence of the overlying mixed layer provides the energy needed to destabilize and erode the underlying stable water mass (Garwood, 1977). Therefore the Turbulent Kinetic Energy (TKE) budget is the basis for the entrainment. This system is closed using a mean-turbulent-field modeling of the vertically integrated equations for the individual TKE components, plus the inclusion of the bulk buoyancy and momentum equations.

Separate vertical and horizontal equations for TKE are used to better model the mixing process. Buoyancy produced energy is somewhat more efficient than shear production as a source of energy for vertical mixing because of its direct effect on the vertical component of the turbulent velocity. The buoyancy equation is generated from the heat and salt equations together with the equation of state:

$$\bar{\rho} = \rho_0\left[1-\alpha\left(\theta-\theta_0\right)+\beta\left(\tilde{s}-s_0\right)\right], \qquad (2-23)$$

and buoyancy is given by:

$$\tilde{b} = g(\rho_0-\tilde{\rho})/\rho_0 \qquad (2.24)$$

where θ is temperature, s is salinity, ρ is density, g is gravity, and the constants α and β are the expansion coefficients for heat and salt. The tilde represents the total instantaneous value and the subscript zero denotes an arbitrary, but representative constant value. Using b instead of $\alpha\,\theta$ for the definition of buoyancy allows this model to be generalized to include salinity.

Temperature and salinity profiles are required as input for model initialization. These are used to compute the mixed layer depth, h. The numerical solution for the NPS mixed layer model defines the minimum mixed layer depth to be 1 m. Other ocean environment parameters to be specified include the fraction of short wave radiation absorbed in the top one meter of the ocean, the radiation extinction coefficient for absorption of radiation with depth, and the critical Richardson number for dynamic stability to be maintained at the bottom of the mixed layer.

The parameters required for surface boundary condition computation include wind speed and direction, cloud cover, sea surface temperature, air temperature, dew-point temperature, incident solar radiation, and the rates of evaporation and precipitation. It should be noted that not all of the incoming short wave radiation penetrates the ocean mixed layer. Approximately half (for open ocean) is absorbed within the first meter. The amount absorbed varies from region to region depending on the amount of absorbing particulates such as phytoplankton and yellow substance. More radiation will be absorbed in coastal regions than in the open ocean region. This portion of absorbed short wave radiation is therefore considered to be part of the upward heat flux.

In a nondimensional context, there will be two degrees of freedom for the dimensionless entrainment flux, $P^*(Z^*,H^*) = -\overline{bw}_{(-h)}h/u_*^3$. The independent parameters are $H^* = h/L_1$ and $Z^* = h/L_2$ where $L_1 = -u_*^3/\overline{bw}(0)$ (the Obokhov length scale) and $L_2 = u^*/f$ (f is coriolis parameter). New ocean mixed layer depth, temperature and salinity are predicted at one hour intervals. The steps in the prediction computation are shown in Figure 7.

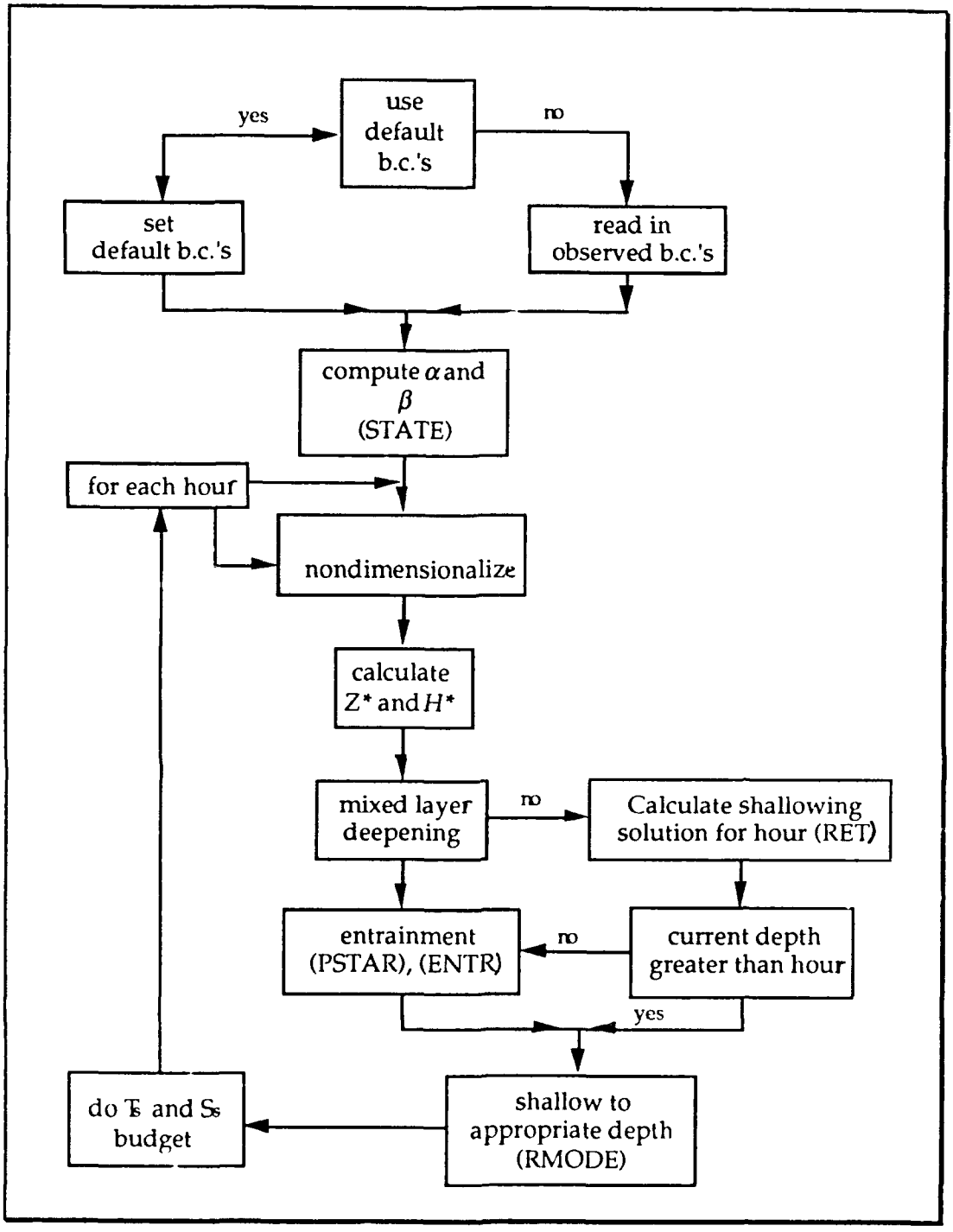

Figure 7. Schematic of Input, Prescription and Computing Steps in NPS Mixed Layer Model Prediction for Each Time Step

V. PROCEDURES, RESULTS AND DISCUSSION

A. PROCEDURE

The aim of this study is to examine the effects of cloud cover and precipitation on the ocean mixed layer. Data collected in 1959 was used in this study. Three experiments with different time scales are designed for this study: namely, short-term experiment (3-day period), medium-term experiment (30-day period) and long-term experiment (365-day period). Each experiment is composed of three different cases (the standard case, Case 1 and Case 2).

In the short-term experiment, the standard case is as follows: the cloud cover is daily mean values of the three-hourly observational data; the precipitation minus evaporation rate ($E\text{-}P_r$) is assumed to be 0.25 cm/day. The case with 20% reduction of cloud cover to the standard case with the same rate of precipitation minus evaporation is taken as Case 1. The case with the same amount of cloud cover as the standard case but with $E\text{–}P_r = 0$ is taken as Case 2 (Table 1). In this experiment we focus on the cloud and precipitation effect on the diurnal variation of the mixed layer depth (MLD) and temperature (T_s).

TABLE 1. SIMULATION CASES FOR THE SHORT-TERM EXPERIMENTS

Month	Days	Standard Case		Case 1		Case 2	
		Cloud Cover (1/8)	P_r-E_v (cm/ day)	Cloud Cover (1/8)	P_r-E_v (cm/ day)	Cloud Cover (1/8)	P_r-E_v (cm/ day)
Jan.	25	7.5	0.25	6	0.25	7.5	0
	26	5.3	0.25	4.2	0.25	5.3	0
	27	7.3	0.25	5.8	0.25	7.3	0
Jun.	156	8	0.25	6.4	0.25	8	0
	157	8	0.25	6.4	0.25	8	0
	158	8	0.25	6.4	0.25	8	0

As for the short-term experiment, three cases are designed for the medium-term experiment, where daily mean value of cloud cover and precipitation are replaced by monthly mean value in the standard case (Table 2). The monthly mean value of cloud cover comes from three-hourly observations while the montly mean value of precipitation are specified by Figure 3.

TABLE 2. SIMULATION CASES FOR THE MEDIUM-TERM EXPERIMENTS

Month	Days	Standard Case			Case 1			Case 2	
		Cloud Cover (1/8)	P_r (cm/ month)	E_v (cm/ month)	Cloud Cover (1/8)	P_r (cm/ month)	E_v (cm/ month)	Cloud Cover (1/8)	P_r-E_v (cm/ month)
Jan.	1-31	6.3	12.5	2.5	5.0	12.5	2.5	6.3	0
Jun.	151-181	7.4	2.8	1.25	5.9	2.8	1.25	5.9	0

Two months that could be characterized as typical, nonetheless produced interesting results. The first is June, where a strong net heat gain ($B_0 > 0$) as

well as a weak wind speed (Figure 20) was noted. Also in January a significant net heat loss ($B_0 < 0$) and stronger wind speed were observed (Figure 16).

As for the long-term (annual) experiment, the time series of changes in MLD and T_s was composed with cloud cover and precipitation variations. Here a complex event with monthly mean value of cloud cover and precipitation (Table 3) will be compared with a simple event using mean yearly value of cloud cover (n = 6.7), precipitation (P_r = 62.2 cm/year), and evaporation(E_v = 48.7 cm/year). Both complex and simple events will be compared with actual bathythermogram(BT) observations. In addition to cloud cover and precipitation, the surface boundary condition including wind direction, wind speed, sea surface temperature, air temperature and dew-point temperature are taken from observational data, which were observed every three hours. The heat and momentum fluxes are computed from these actual observations. The initial temperature profile is selected from one of 665 BT measurements. This temperature profile plus observed precipitation and calculated evaporation were used as initial condition of the model. In these experiments, the standard case (subscript 0) will be compared with Case 1 (subscript 1) and Case 2 (subscript 2). When subtracting the results of Case 1 and Case 2 by standard case, the differential values provide:

1. Differential MLD ($H_0 - H_1$) and differential T_s ($T_{s0}-T_{s1}$) in variable cloud simulation.
2. Differential MLD ($H_0 - H_2$), differential T_s ($T_{s0} - T_{s2}$) and differential salinity ($S_0 - S_2$) in variable precipitation simulation.

The working hypothesis here is that cloud cover change will make sea surface temperature change, which will lead to mixed layer and boundary condition changes. Thus, the MLD and T_s prediction will become more

complicated. In order to simplify the problem, we assume all boundary variables were constant except cloud cover and precipitation in these experiments.

TABLE 3. SIMULATION CASES FOR THE LONG-TERM EXPERIMENT (COMPLEX EVENT)

Month	Days	Standard Case			Case 1			Case 2	
		Cloud Cover (1/8)	P_r (cm/ month)	E_v (cm/ month)	Cloud Cover (1/8)	P_r (cm/ month)	E_v (cm/ month)	Cloud Cover (1/8)	P_r-E_v (cm/ month)
Jan.	1-31	6.3	12.5	2.5	5.0	12.5	2.5	6.3	0
Feb.	32-59	5.9	2.5	4.8	4.7	2.5	4.8	5.9	0
Mar.	60-90	6.8	7.5	3.8	5.4	7.5	3.8	6.8	0
Apr.	91-120	6.5	2.5	1.3	5.2	7.5	1.3	6.5	0
May	121-151	7.3	2.5	1.9	5.8	2.4	1.9	7.3	0
Jun.	152-181	7.6	2.8	1.25	5.9	2.8	1.25	7.4	0
Jul.	182-212	7.6	5.0	1.2	6.1	5.0	1.2	7.6	0
Aug.	213-243	7.4	4.4	2.5	5.9	4.4	2.5	7.4	0
Sep.	244-273	6.6	2.5	3.0	5.3	2.5	3.0	6.6	0
Oct.	274-304	6.3	8.8	5.0	5.0	8.8	5.0	6.3	0
Nov.	305-334	6.2	5.6	6.9	6.9	5.6	6.9	6.2	0
Dec.	335-365	5.8	5.6	15.0	4.6	5.6	15.0	5.8	0

B. RESULTS AND DISCUSSION

1. Short-Term Experiments

Two events were extracted from the months of January and June. These events were chosen at random, and as such, do not represent

exceptional or special cases. Diurnal variation of MLD, T_s and mixed layer salinity were examined in these periods.

a. Event #1 (January, days 25-27)

The wind speed was low at the beginning of the event and later reached its maximum speed in the middle of the second day (Figure 8a). The model simulation began an hour before sunset. The initial MLD was not deep (45 m) when compared to the typical MLD in January. The net surface heat flux indicated a net heat loss during this period (Figure 8b). Figure 9 shows the variation of differential MLD and T_s in the variable cloud simulation. The differential MLD was negative during each night and positive during each daylight period. The maximum negative differential MLD occurs after midnight of the first day due to a lull in the wind velocity. A near zero differential MLD appeared the second day in association with the onset of stronger winds. The key to examining this phenomenon is the disproportionate darkness of the long January nights (~16 hours). The greenhouse effect was particularly active during the lengthy hours of darkness, resulting in pronounced long-wave radiation return back to the ocean surface in the standard case, thereby producing a shallower MLD.

After the sun rise, the albedo effect dominated variations of the MLD when the surface buoyancy flux was downward. Then, due to a net increase in solar radiation reaching the ocean surface in Case 1, the interaction of these dynamics leads to a shallower MLD than would be found in the standard case.

The significant greenhouse effect throughout the hours of darkness will result in a warming of the ocean surface, a form of positive

differential T_s. Negative differential T_s, found during daylight hours, were associated with the deeper MLD of the standard case. The maximum differential of T_s occurred toward the end of daylight on the first day when the MLD was shallow.

Unlike the variations in differential MLD and T_s found in the variable cloud simulation, the differential MLD and T_s in the variable precipitation simulation produced consistently negative values throughout the period (Figure 10). The influx of fresh water into the mixed layer will result in a shallower MLD, ultimately producing a lower mixed layer temperature associated with a net heat loss in this period. Again, the maximum negative differential MLD and T_s noted during the variable precipitation simulation are associated with a lull in the wind occurring during the hours of darkness on the first day. The differential of mixed layer salinity increased in a stepwise manner throughout the period (Figure 11a). It should be noted that variations in differential salinity are dependent upon variable wind velocities, i.e. in the case of $E-P_r < 0$, an increase of wind velocity will entrain saline water from the lower layers into the mixed layer, thereby increasing the mixed layer salinity and decreasing the differential salinity.

Comparing the mean value of MLD and T_s in this event (see Table 4), two features arise worthy of note. For the first, when we compare the difference in mean MLD between the standard case and Case 1 (~0.3 m), the difference is strikingly less than what appears in a comparison of the standard case and Case 2, when a differential of about 4 m is found. The implication is that precipitation has had a significant and pronounced effect

upon the MLD during this event. Secondly, we may note that due to a deeper MLD and weaker solar radiation, the mean value of T_s has nearly no change throughout the period.

TABLE 4. THREE-DAY MEAN VALUES OF MLD, TEMPERATURE, NET SURFACE HEAT FLUX AND MIXED LAYER SALINITY

Event	Days	Case	$\overline{H}$ (m)	$\overline{T}_s$ (°C)	$\overline{Q}_0$ (w/m²)	$\overline{S}$ (PPT)
January	25	Standard	45.5	5.4	33.8	31.9
	∫	1	45.9	5.4	32.9	31.9
	27	2	49.6	5.4	33.8	32.0
June	156	Standard	36.1	7.6	–73.4	31.9
	∫	1	32.4	7.5	–160.9	31.9
	158	2	37.1	7.6	–73.4	32.0

b. Event #2 (June, days 156-158)

In this event the MLD is approximately 40 m, and the downward buoyancy flux was stronger than event #1. The wind was more pronounced at the beginning of the event but subsequently decreased from the middle of the first day (Figure 12). Daylight and the associated period of insolation comprised 13 hours. The model simulation began in the afternoon, four hours before sunset.

The differential MLD and T_s in the variable cloud simulation are displayed in Figure 13. At the beginning of the event, a stronger wind and weak upward buoyancy flux lead to a near-zero differential MLD and T_s during the hours of darkness of the first day. Then as conditions change, the

positive differential MLD and the negative differential T_s increased during the day and diminish in the darkness. This pattern indicates that the albedo effect has significant influence on MLD and T_s during any day having strong solar radiation and a lengthened duration of insolation. In the standard case, the clouds scatter and absorb a significant amount of incoming solar radiation, decreasing the downward buoyancy flux at the ocean surface during the day. This decrease in the downward buoyancy flux will, in turn, lead to an increase in entrainment velocity thereby deepening the mixed layer and cooling the ocean surface. The greenhouse effect had little significant impact on the mixed layer during the period of this event due to relative decrease in the hours of darkness and weaker long wave radiation.

The differential MLD produced negative values in the variable precipitation simulation (Figure 14a). The precipitated fresh water has the effect of increasing stratification of the upper ocean in the standard case. As the stratification becomes more pronounced, so does the density jump at the base of the mixed layer, resulting in a decrease in the rate of entrainment. With the decrease in the rate of entrainment, the MLD then retreated relative to the case of $E-P_r = 0$. A positive differential T_s is associated with a shallower MLD in the standard case (Figure 14b). The variation in differential salinity grew in stair-step fashion throughout the period of the event. (Figure 11b).

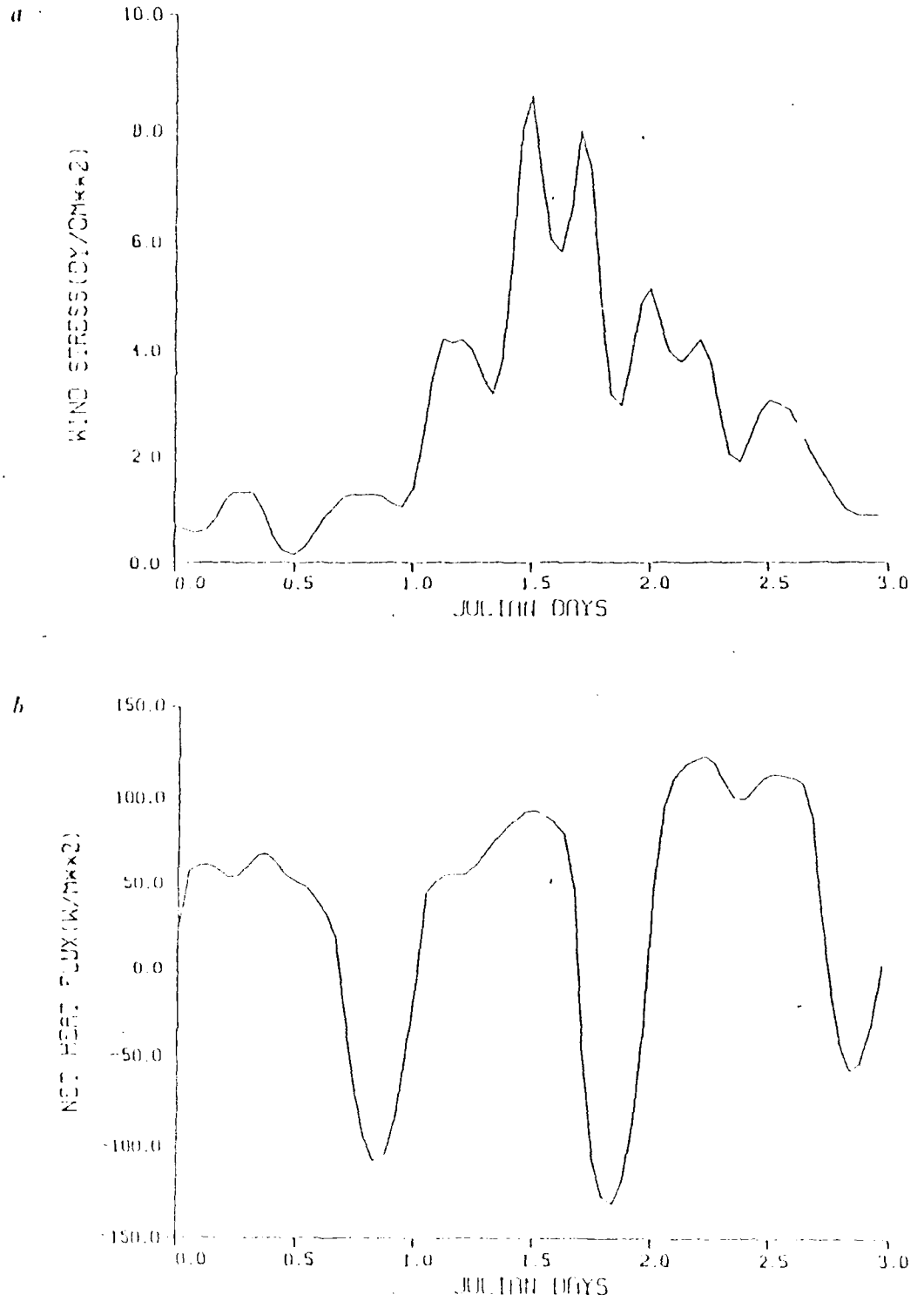

Figure 8. Variation of (a) Wind Stress and (b) Net Surface Heat Flux (January, days 25-27)

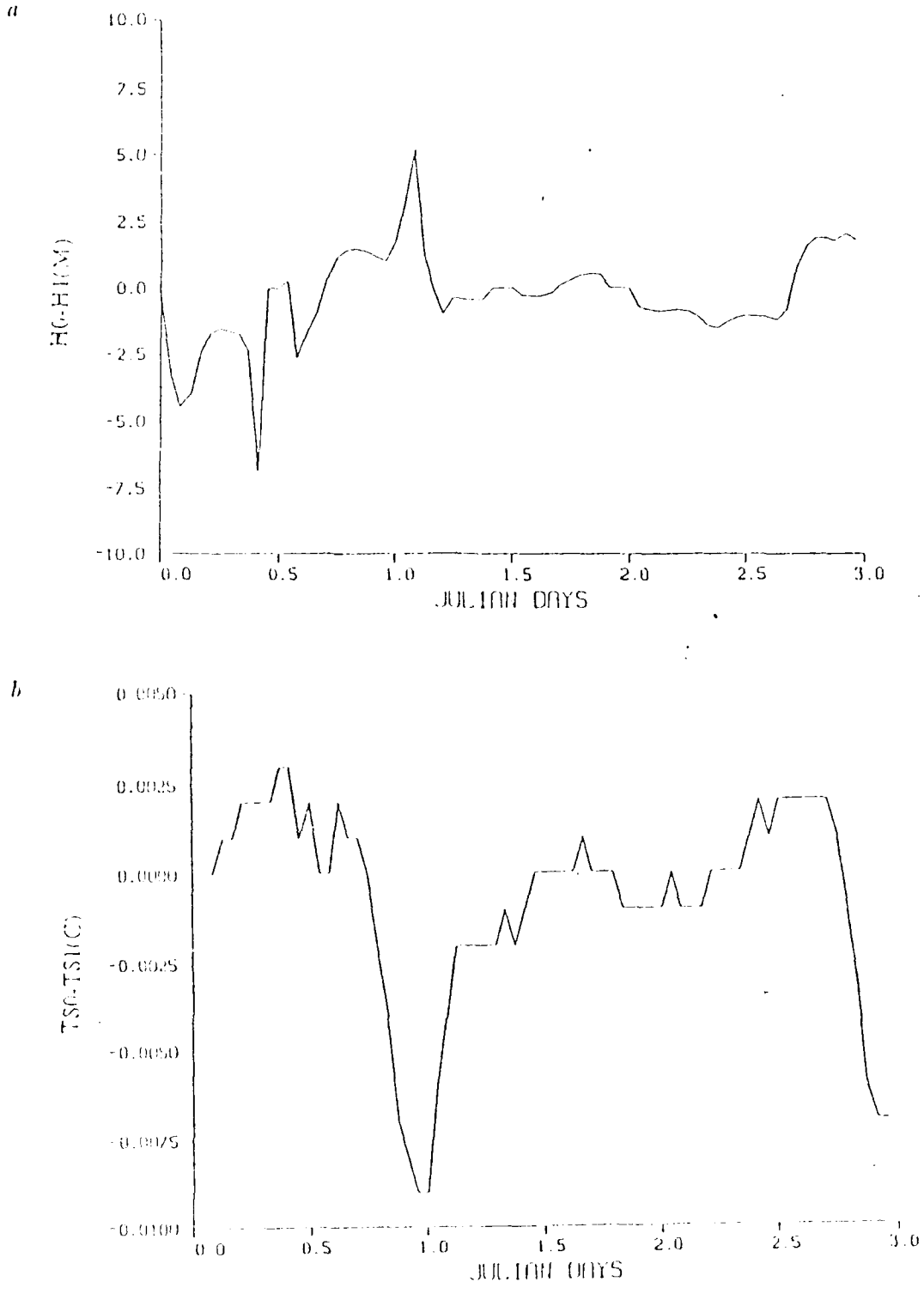

Figure 9. Variation of (a) Differential MLD and (b) Differential T_s in the Variable Cloud Simulation (January, days 25-27)

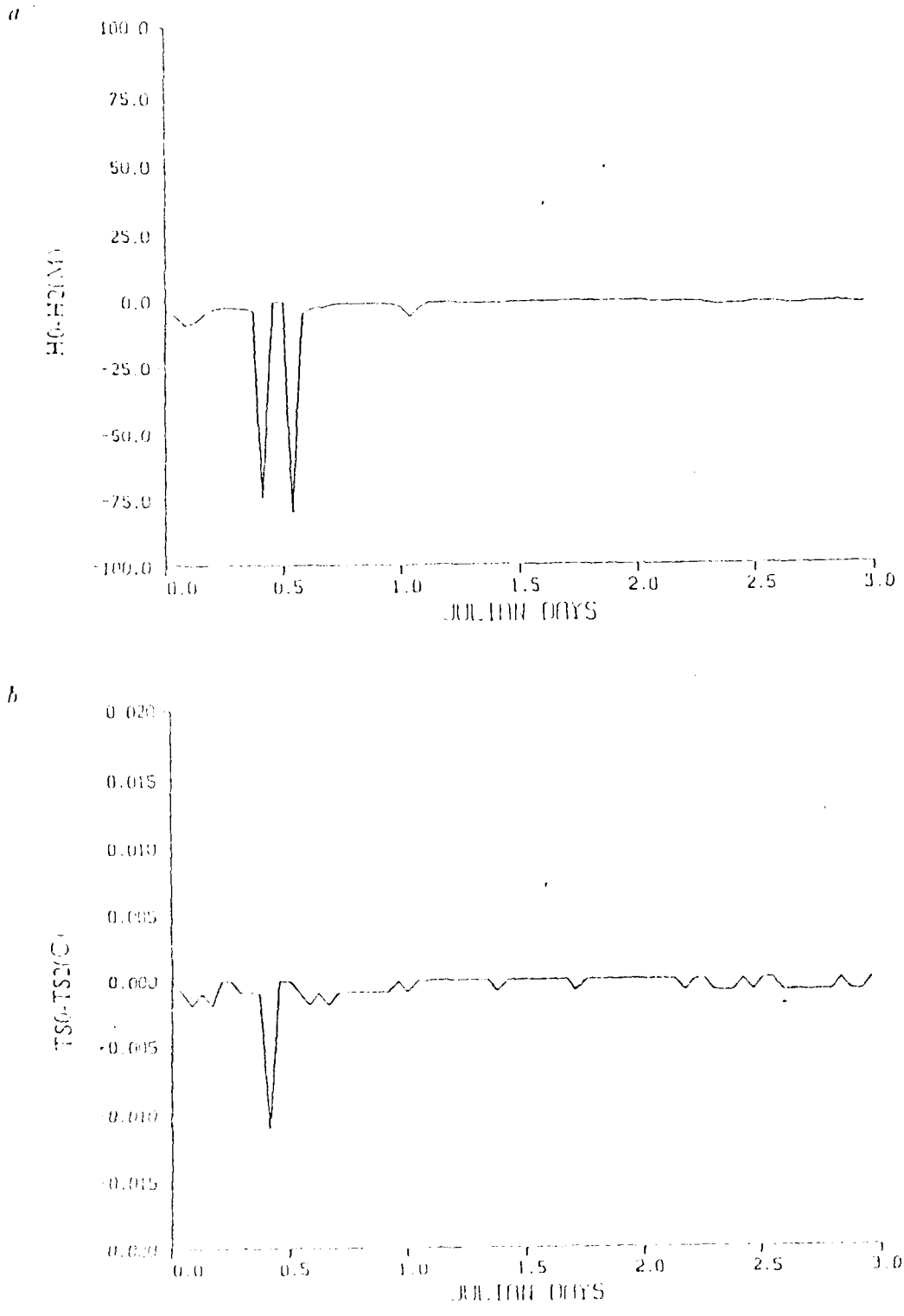

Figure 10. Variation of (a) Differential MLD and (b) Differential T_s in the Variable Precipitation Simulation (January, days 25-27)

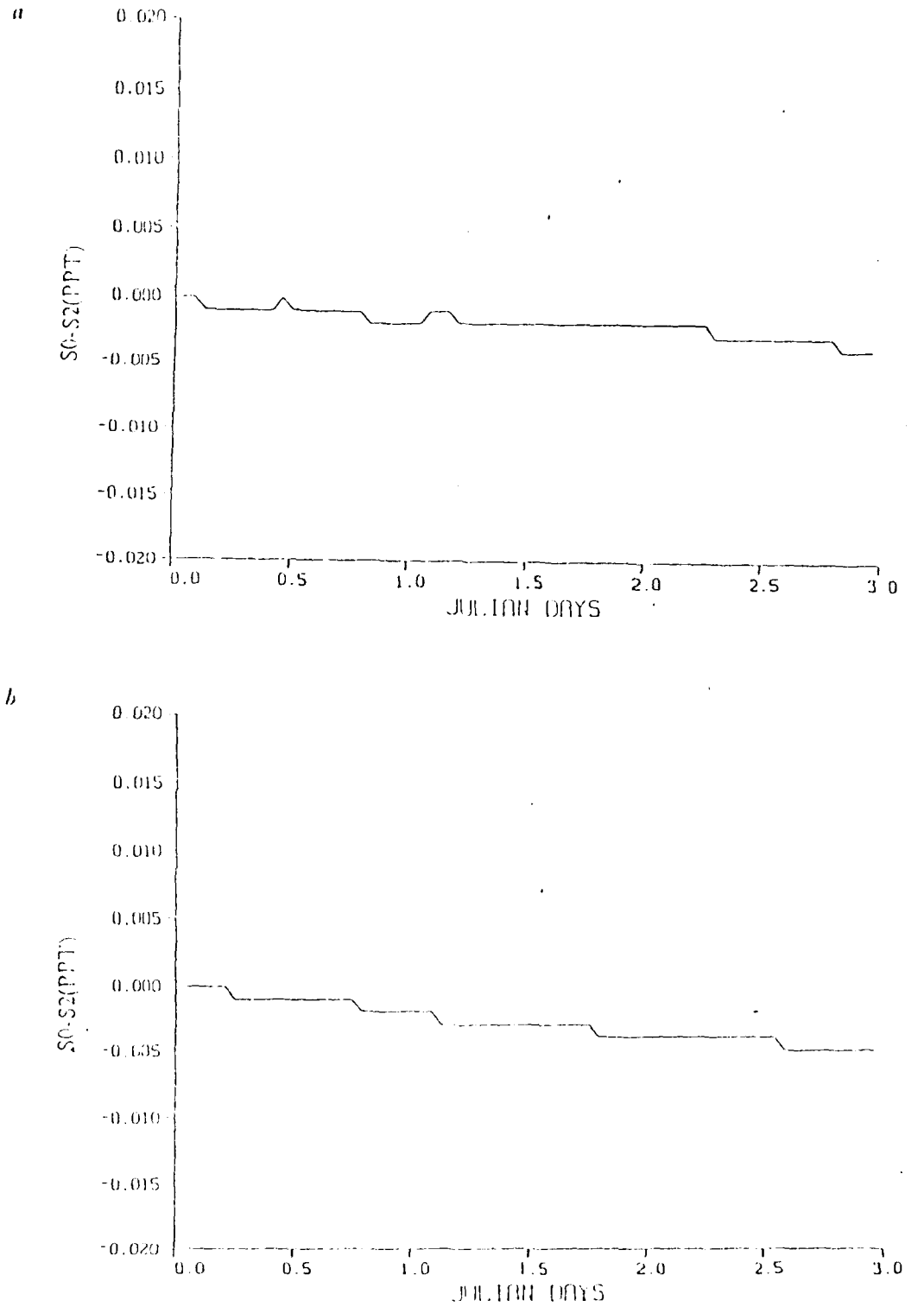

Figure 11. Variation of Differential Salinity in (a) Event #1 and (b) Event #2 for the Short-term Experiment

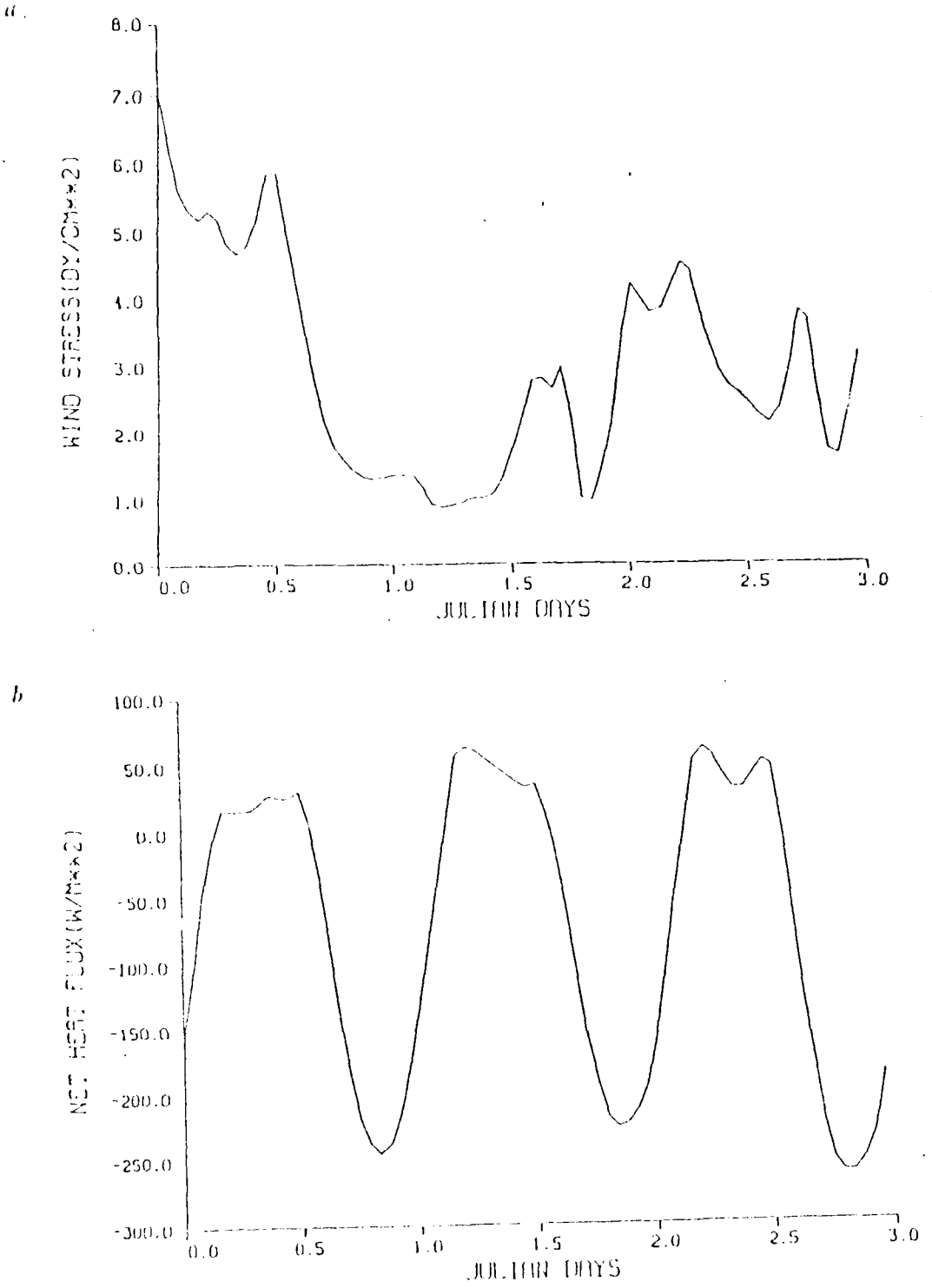

Figure 12. Variation of (a) Wind Stress and (b) Net Surface Heat Flux (June, days 156-158)

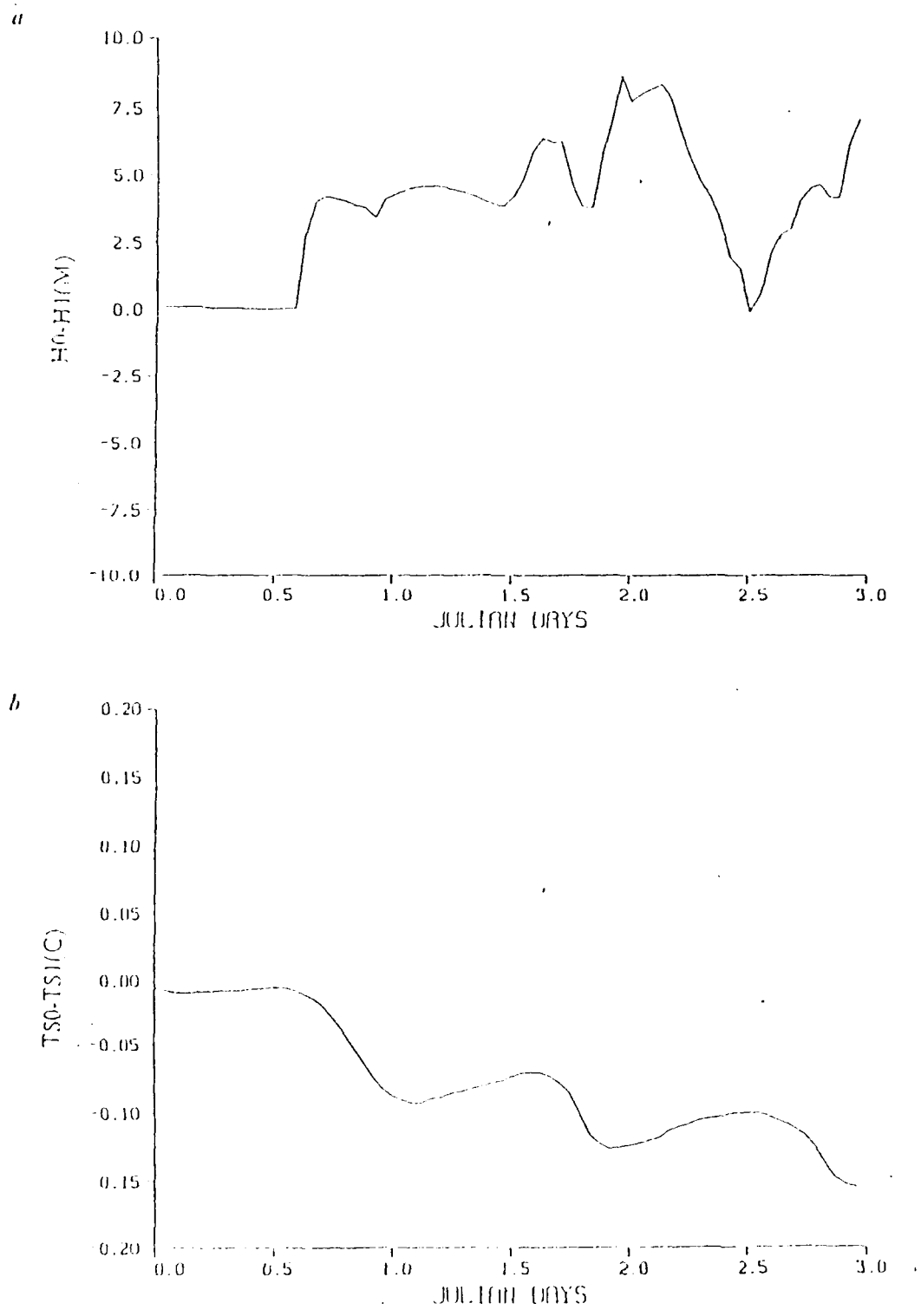

Figure 13. Variation of (a) Differential MLD and (b) Differential T_s in the Variable Cloud Simulation (June, days 156-158)

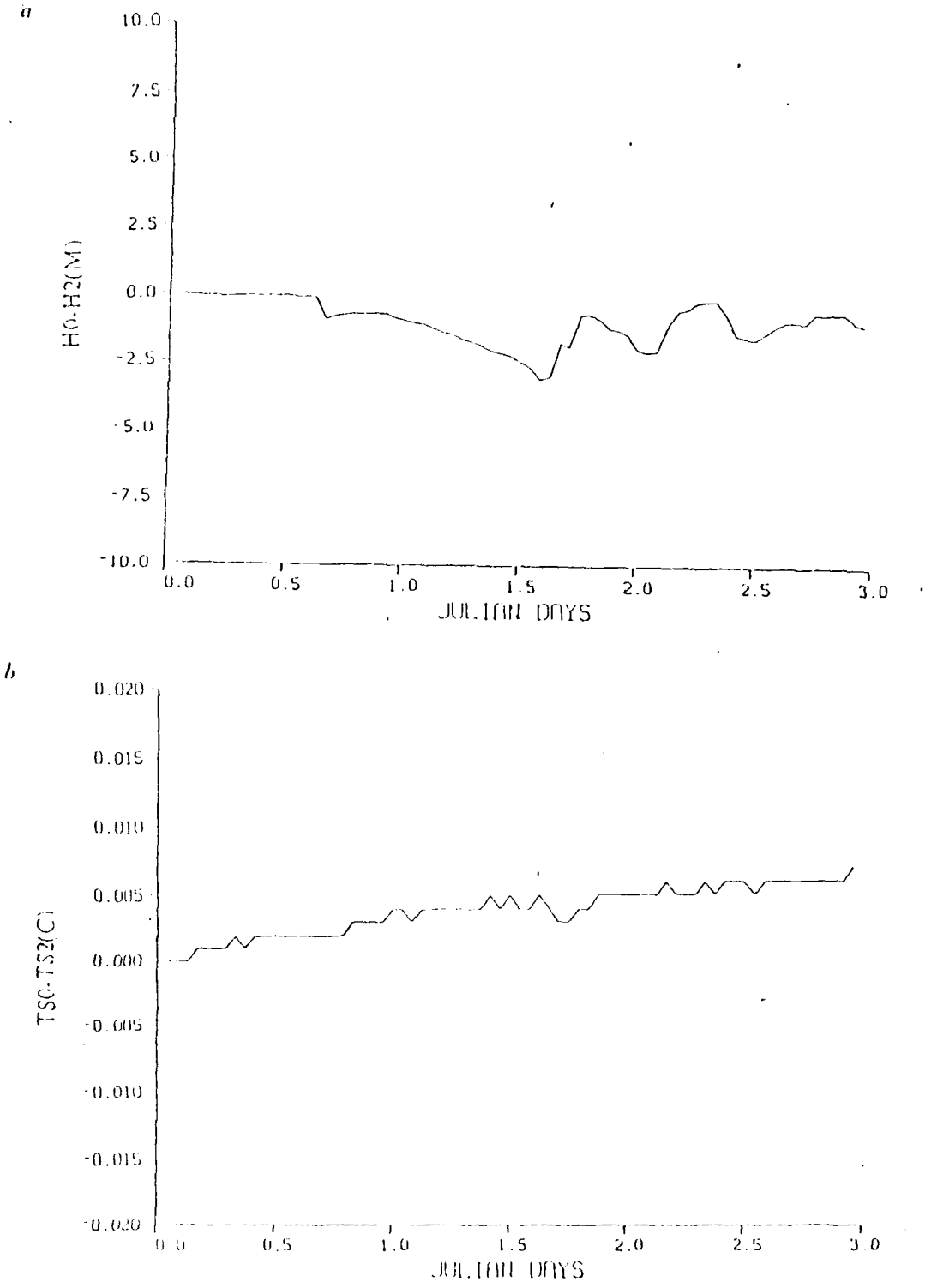

Figure 14. Variation of (a) Differential MLD and (b) Differential T_s in the Variable Precipitation Simulation (June, days 156-158)

Examining the mean value of the net surface heat flux (see Table 4), we find a significant difference between the standard case and Case 1 during the event. The mean surface heat flux shows a large increase, 87.5 w/m^2 in this event, compared to 0.9 w/m^2 in Event #1. This indicates that the clouds have significant impact on surface buoyancy flux and directly influence upper ocean dynamics during this event. Another striking feature that arises from the figures in Table 4 is the difference of mean MLD between the standard case and Case 2 (0.9m) that is distinctly less than those of Event #1 (4.008m). These figures illustrate that the dynamic effect of precipitation on MLD was greater for the circumstances of Event #1.

2. Medium-term Experiments

a. January (days 1-31)

In general, the MLD is deeper than the annual average in this period, subject to interaction with strong winds and strong upward buoyancy flux (Figures 15a and 16). The model simulation began at an hour before dark.

The variation of differential MLD in the variable cloud simulation produced a positive differential MLD during the day and a negative differential MLD during the night (Figure 17a). This result is similar to the results found in the short-term experiment of Event #1, where the greenhouse effect is the dominant factor on the MLD during the night while the albedo effect became the significant factor during the day, associated with a downward buoyancy flux. A larger differential MLD than what might otherwise be expected is a reflection of a lull wind which can serve to either deepen or shallow the MLD.

With the exception of a few negative differential T_s's occurring in daytime, and which are essentially anomalies, the differential T_s was generally positive throughout the period (Figure 17b). Varying consistently with the diurnal cycle, decreasing differential Ts correlated with daylight. Differential Ts increased consistently with night. The differential Ts in this circumstance is a clear reflection of the predominant greenhouse effect in January. The stronger upward buoyancy flux associated with the mid-latitude winter regime will result in a colder ocean surface in Case 1 as more long wave radiation escapes from the ocean surface. In the case of shallower MLD in daylight hours due to weaker wind velocity, the ocean surface in Case 1 may become warmer and form a negative differential T_s.

The variation of differential MLD and T_s in the variable precipitation simulation are displayed in Figure 18. As a result of precipitation damping turbulent kinetic energy and consequently inducing the MLD to become shallower in the standard case, a negative differential MLD appears throughout the period. The shallower MLD in the standard case then lost more upward long wave radiation, and caused ocean surface to be colder than is the case with $E-P_r = 0$. Quite predictably, a negative differential T_s also appeared throughout the period. There was one exception to this otherwise rigid pattern, however. During the daylight hours of the day 16, a single instance of positive differential T_s occurred due to the shallowest MLD that developed during the period, which increases the mixed layer temperature in the standard case. A striking variation in differential salinity also occurred on day 16 while the MLD was at its shallowest (Figure 19a).

b. June (Days 152-181)

Except for a storm that occurred on the second day of the month, the winds were moderate until the middle of the month and minimal afterwards (Figure 20a). The value of net surface heat flux indicate a strong downward buoyancy flux at the ocean surface during the period (Figure 20b). The MLD was approximately 35m at the beginning of the period and correspondingly decreased after day 13 as wind velocities began to subside (Figure 15b). The model simulation began in the afternoon, four hours before darkness.

Figure 21 shows the variation of differential MLD and T_s in the variable cloud simulation. Prior to day 13, a few hours of negative differential MLD occurred in the hours of darkness. But after day 13, the differential MLD became consistently positive and established a pattern of variation in strict conformance with variations in wind magnitude, higher wind velocities increasing the differential MLD. This indicates that the albedo effect dominates the variation of MLD in June, associated with a typical mid-latitude summer regime (i.e. strong solar radiation and longer insolation duration).

The negative differential T_s also kept a constant value before day 13 when the MLD was relatively deeper. The maximum differential T_s (in excess of 4°C) is reached on the day 27 when the MLD becomes quite shallow (<5m). This sequence suggests that the cloud effect on mixed layer temperature is particularly dramatic when the mixed layer is very shallow. After day 27, the MLD deepens again due to increasing wind velocity, and the differential T_s therefore decreased to near zero.

The variation of differential MLD and T_s in the variable precipitation simulation is shown in Figure 22. Similar to result showed in January, the negative differential MLD appeared throughout the period, but the magnitude of the differential was less than what occurred in January due to a smaller quantity of precipitation in June (see Table 2). Associated with the negative differential MLD there is a positive differential T_s which holds a constant value close to zero preceding day 13, and then rapid increase on the seventeenth and twenty-ninth days when the MLD becomes very shallow. A similar pattern of occurrence also has been found in the differential salinity variation (Figure 19b). This is consistent with the fact that a shallow MLD may lead to an increase of variability for both temperature and salinity within the mixed layer.

The mean value of MLD, T_s, net surface heat flux and mixed layer salinity for January and June are shown in Table 5. These values would indicate that the effects of the clouds and precipitation will result in interactive dynamics on the mixed layer that differ with the seasons. First, the difference in mean MLD between the standard case and Case 1 in June (2.34m) is greater than that of January (0.56m), but the difference in mean MLD between the standard case and Case 2 in June (0.26m) is significantly less than that found in January (7.39m). The demonstrated variation in these results suggest that the clouds have the greatest impact on MLD in June, while the effects of precipitation were obviously more significant in January.

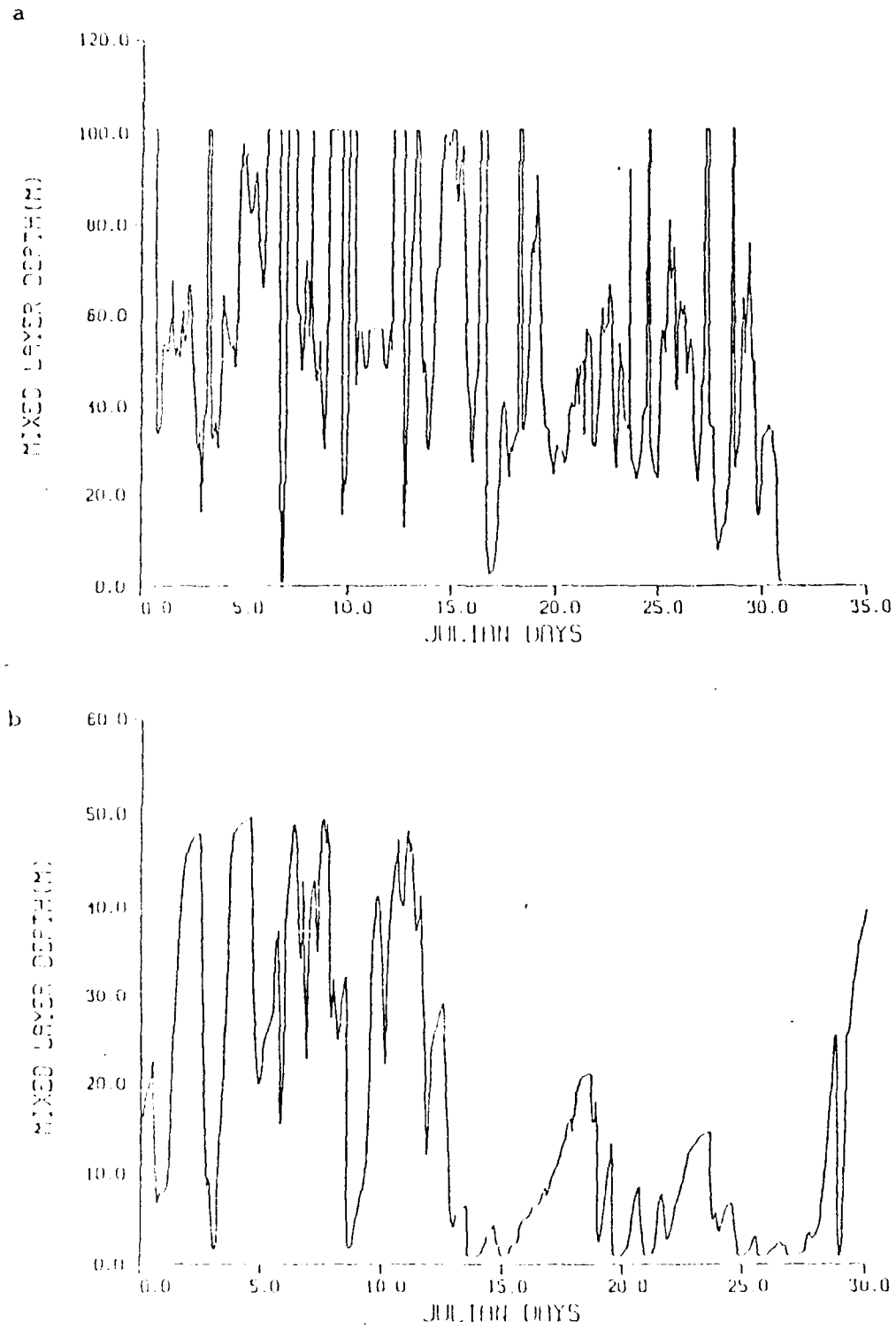

Figure 15. Variation of MLD in (a) January and (b) June in the Standard Case

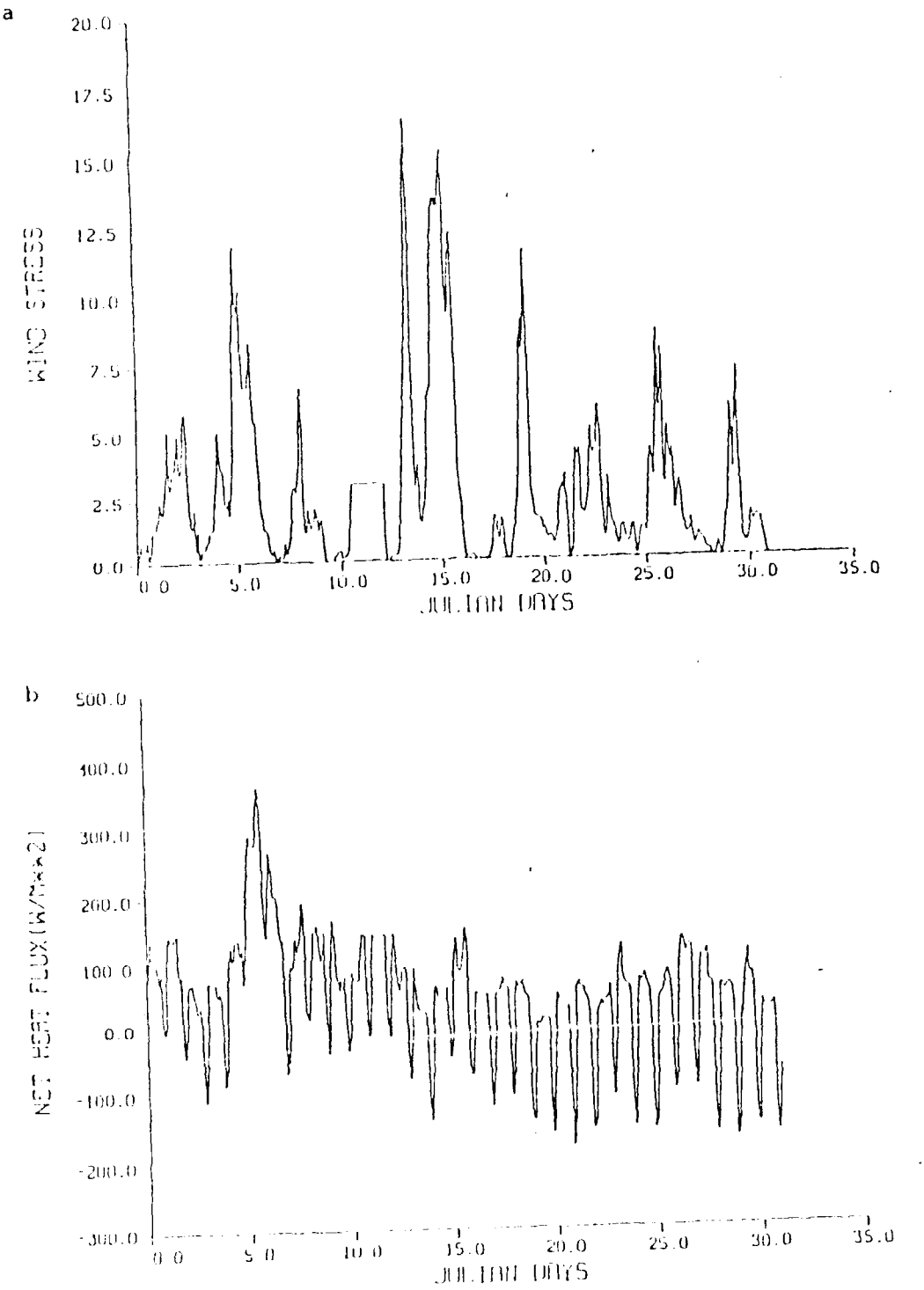

Figure 16.. Variation of (a) Wind Stress (b) Net Surface Heat Flux in January

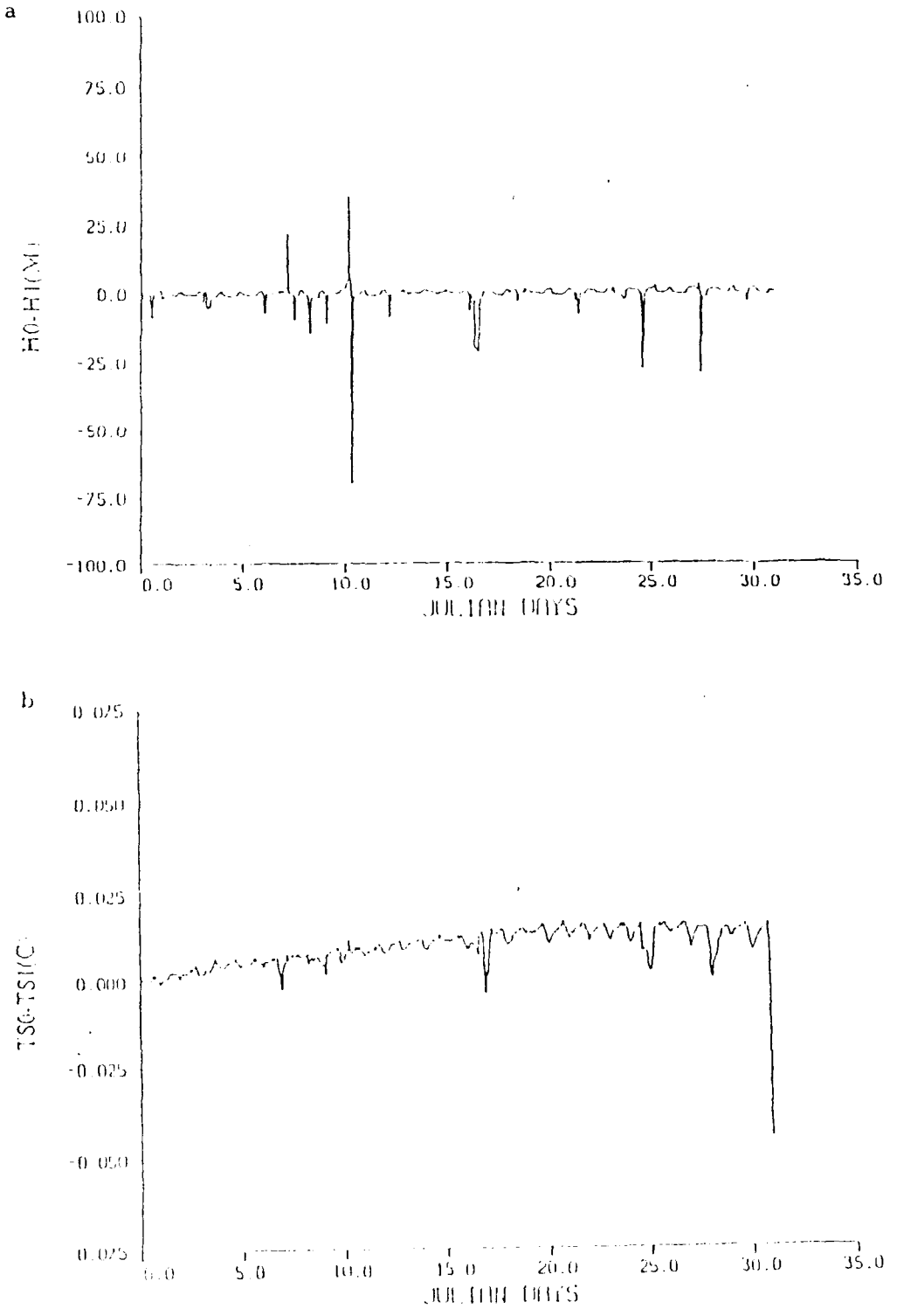

Figure 17. Variation of (a) Differential MLD and (b) Differential T_s in the Variable Cloud Simulation in January

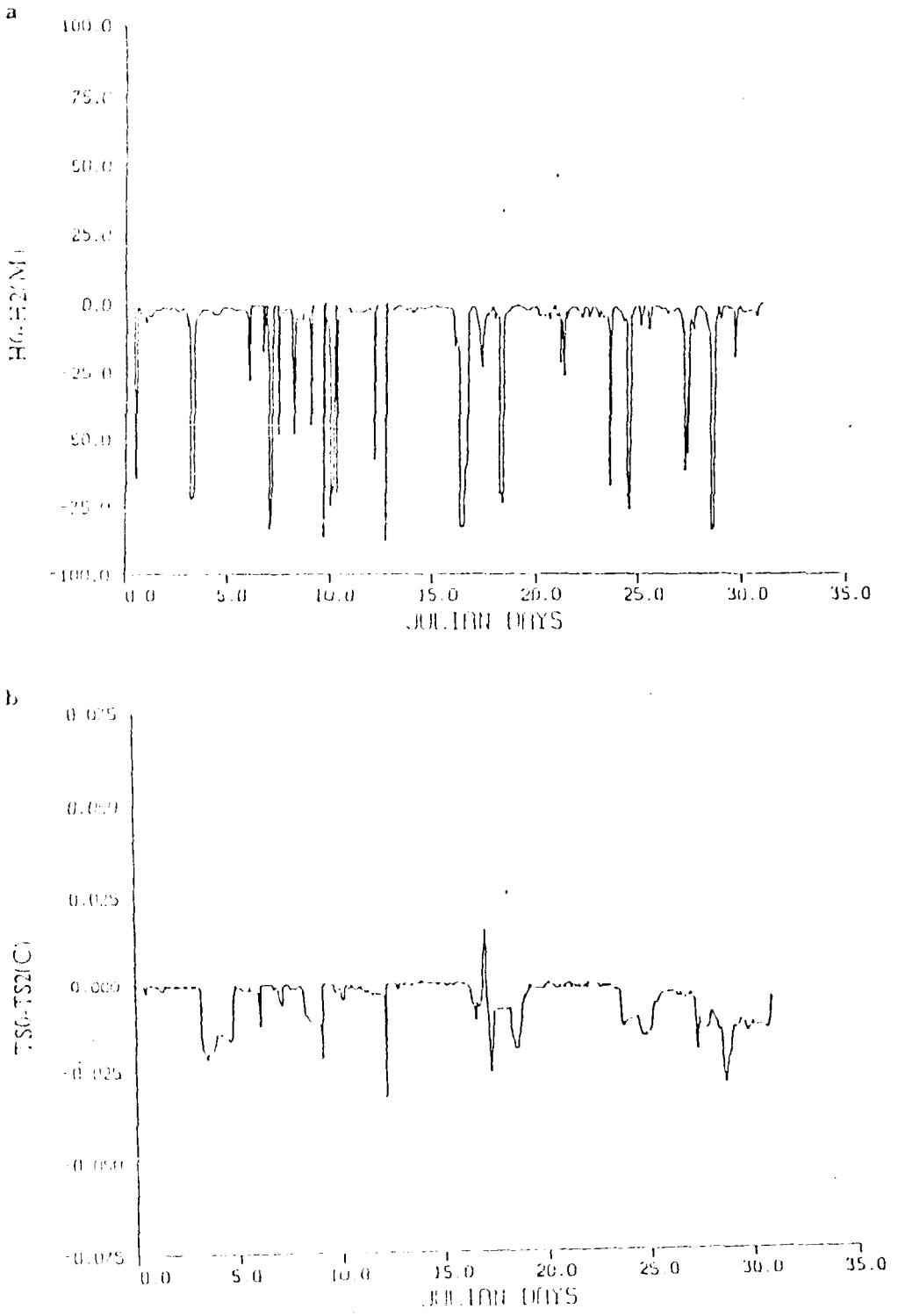

Figure 18. Variation of (a) Differential MLD and (b) Differential T_s in the Variable Precipitation Simulation in January

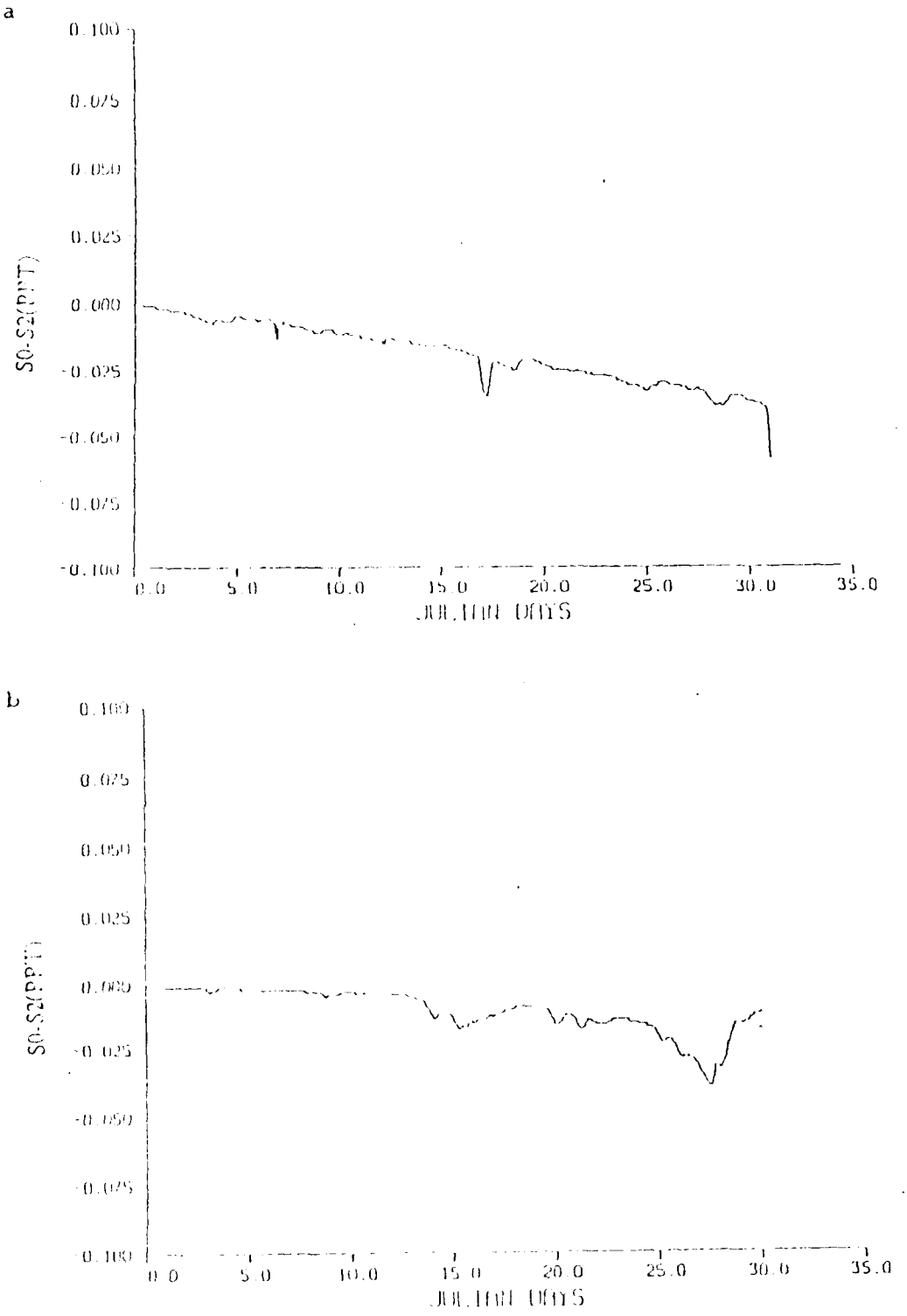

Figure 19. Variation of Differential Salinity in (a) January and (b) June

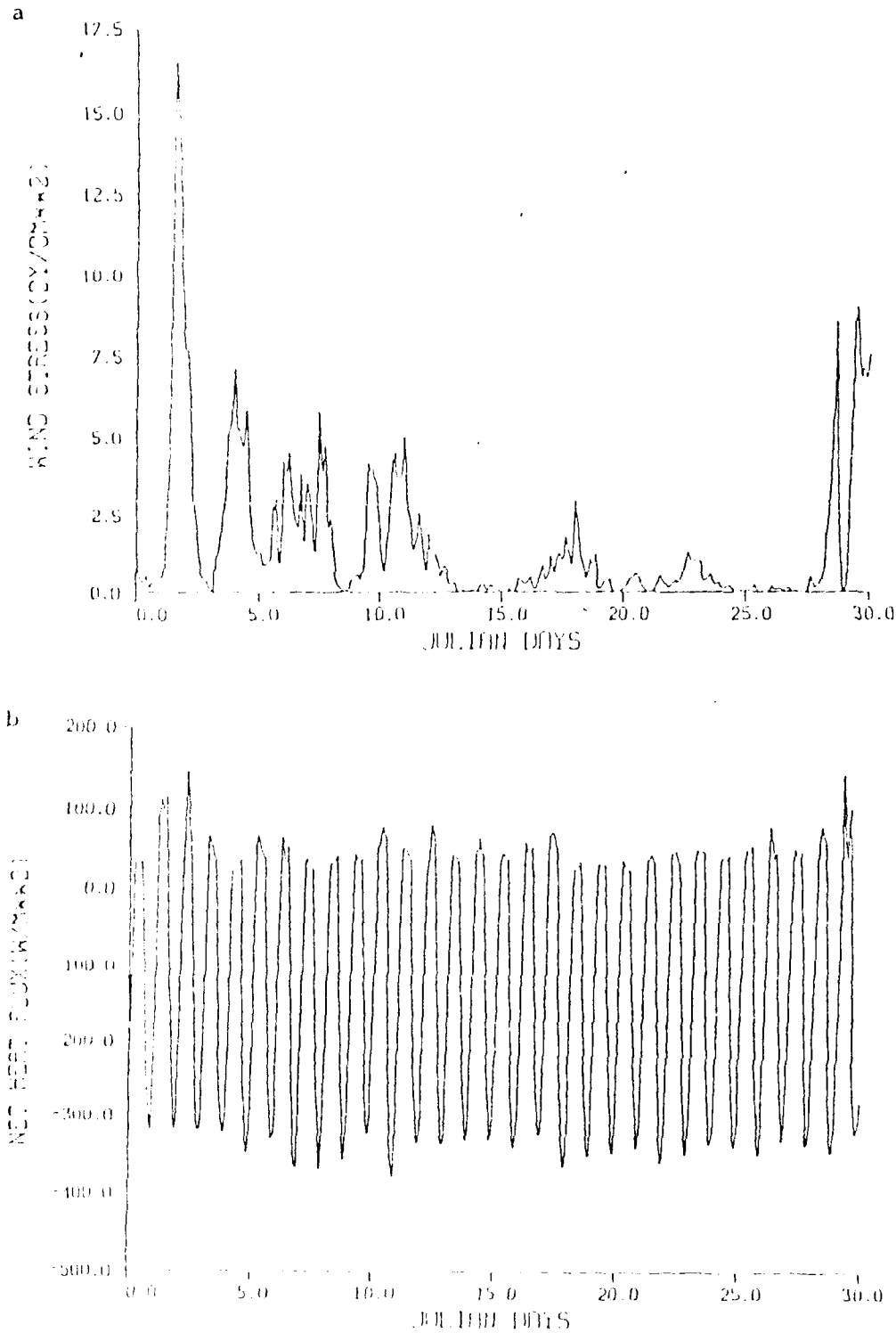

Figure 20. Variation of (a) Wind Stress and (b) Surface Net Heat Flux in June

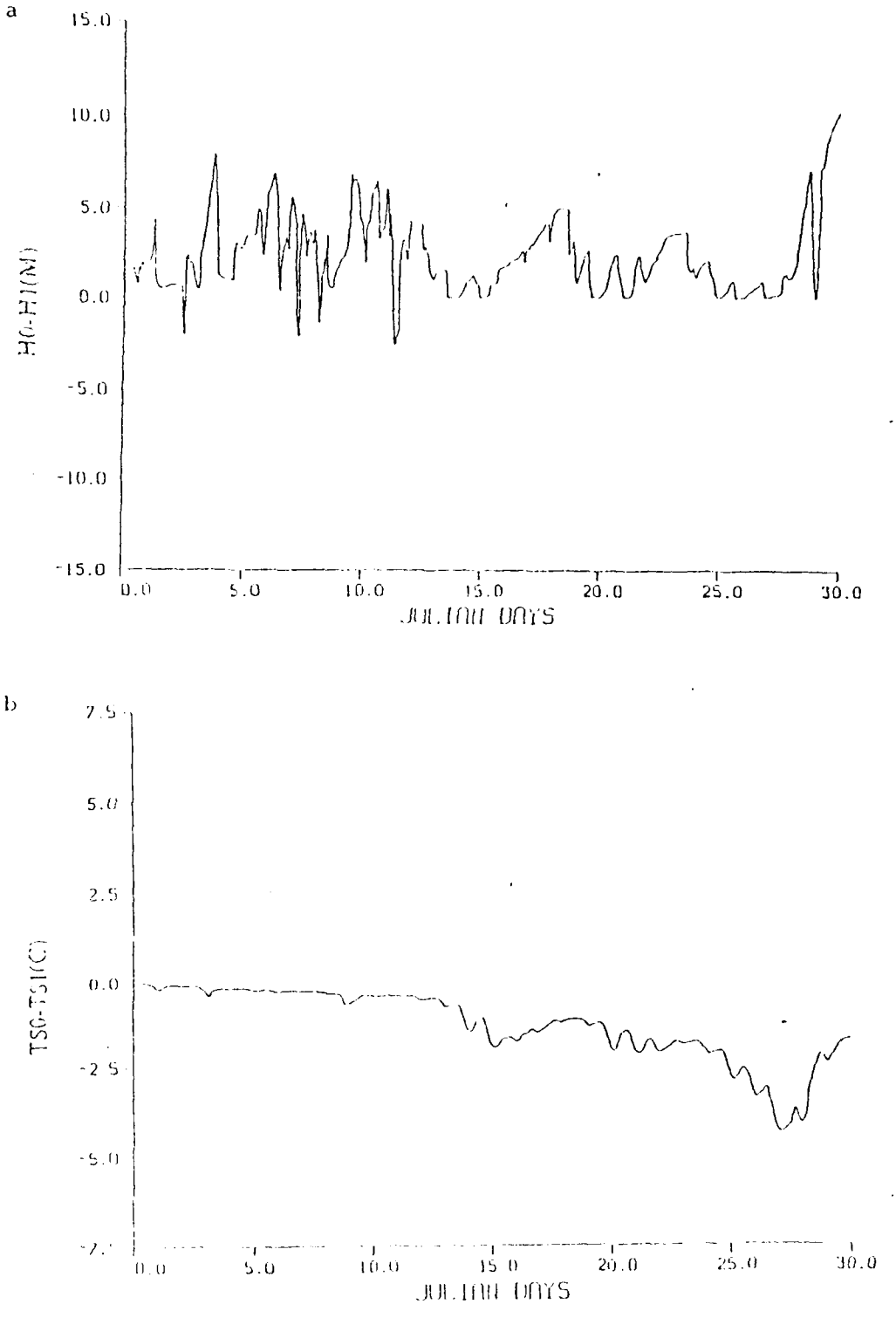

Figure 21. Variation of (a) Differential MLD and (b) Differential T_s in the Variable Cloud Simulation in June

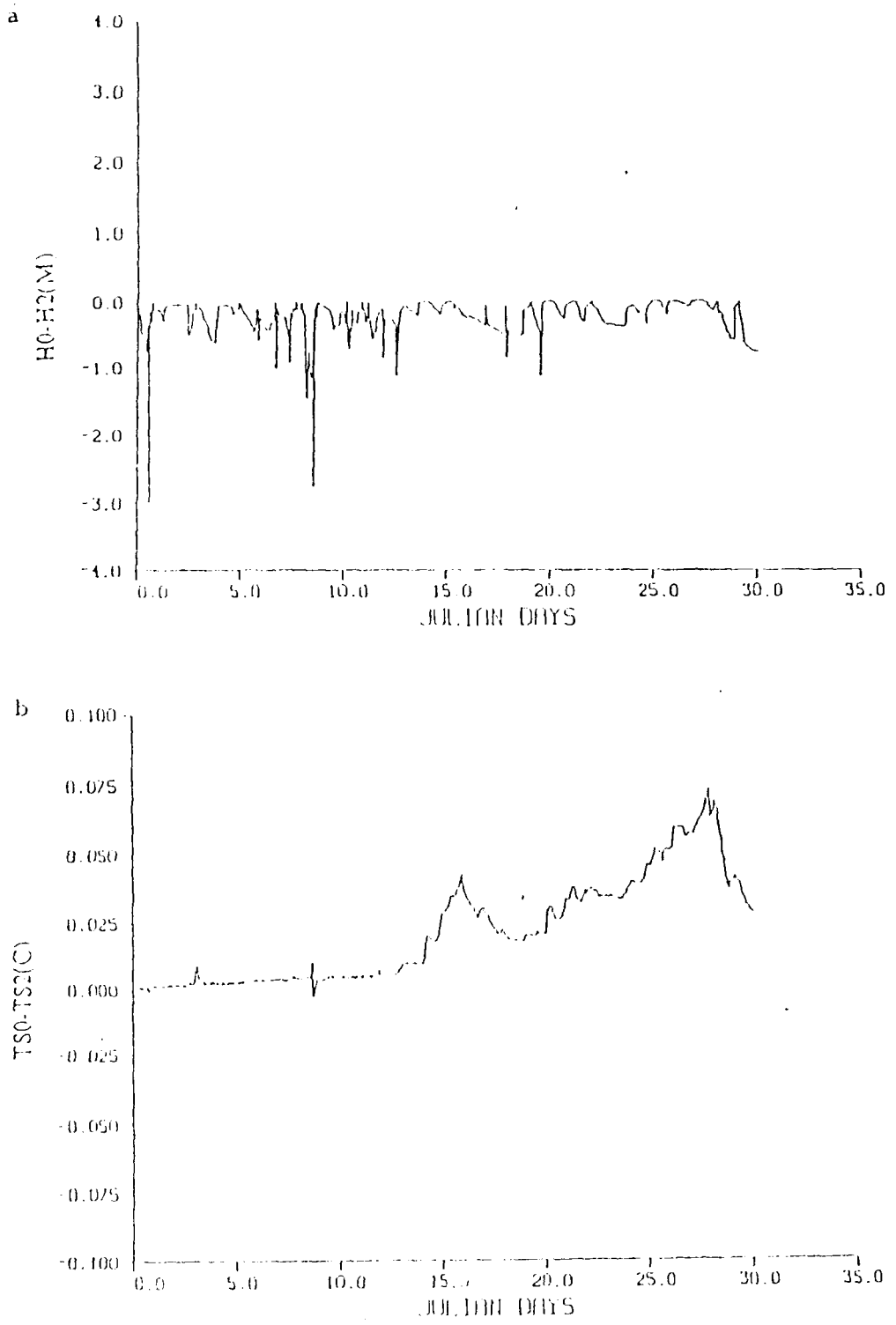

Figure 22. Variation of (a) Differential MLD and (b) Differential T_s in the Variable Precipitation Simulation in June

TABLE 5. MONTHLY MEAN VALUES OF MLD, TEMPERATURE, NET SURFACE HEAT FLUX AND MIXED LAYER SALINITY

Event	Days	Case	$\overline{H}$ (m)	$\overline{T}_s$ (C)	$\overline{Q}_0$ (w/m^2)	$\overline{S}$ (PPT)
January	1	Standard	49.0	5.9	49.2	31.9
	∫	1	49.6	5.9	51.2	31.9
	31	2	56.4	5.9	49.2	32.0
June	152	Standard	17.1	9.2	−109.4	31.9
	∫	1	14.7	10.5	−179.3	31.9
	181	2	17.3	9.2	−109.4	32.0

Second, the positive mean net surface heat flux indicates a net heat loss at the ocean surface in January, while a negative mean net surface heat flux in June denotes a net heat gain. A pronounced net heat loss will cause the MLD of Case 1 to be deeper than the MLD of standard case due to the lessening of the greenhouse effect. A reverse effect occurs as significant net heat gain leads to a shallower MLD in Case 1 than in the standard case as the albedo effect becomes enhanced in the standard case. Another meaningful index of seasonal tendencies is the very large difference between the mean net surface heat flux recorded in June (69.8 w/m^2) and the substantially smaller figures of January (2.1 w/m^2). The implication of this large difference is that variations of the clouds in June dominate the strength of surface buoyancy flux and directly influences mixed layer dynamics.

3. Long-Term Experiments

A mixed layer simulation of 365 days was conducted in order to examine the cumulative and serial effects of cloud cover and rainfall events over time. Monthly mean value of cloud coverage and precipitation are available for what we have termed the "complex" event, and the annual

mean value of cloud coverage and precipitation are used for a "simple" event. Comparing these two events, we find some distinctions in the MLD, temperature and salinity prediction between the two events. The output of the MLD and temperature from the complex and simple events are compared to BT observations.

a. Complex Event

During the annual cycle of the sea surface temperature, the ocean surface warms from April through September and cools during the remaining months. The time series of yearly variations in net heat flux (Figure 23a) corresponds to this annual cycle. Also associated with the annual cycle there is a pronounced downward buoyancy flux in the warming season, followed by a shift to an upward buoyancy flux as the ocean surface cools. The annual variation of surface wind stress is shown in Figure 24. Cloud cover is relatively diminished during the cooling season, while cloudy days frequently appear in the warm season (Figure 4). These atmospheric boundary conditions are in concourse with a deepening of MLD and lower mixed layer temperature during the cooling season and a shallower MLD and higher mixed layer temperature during the warming season (see dotted line in

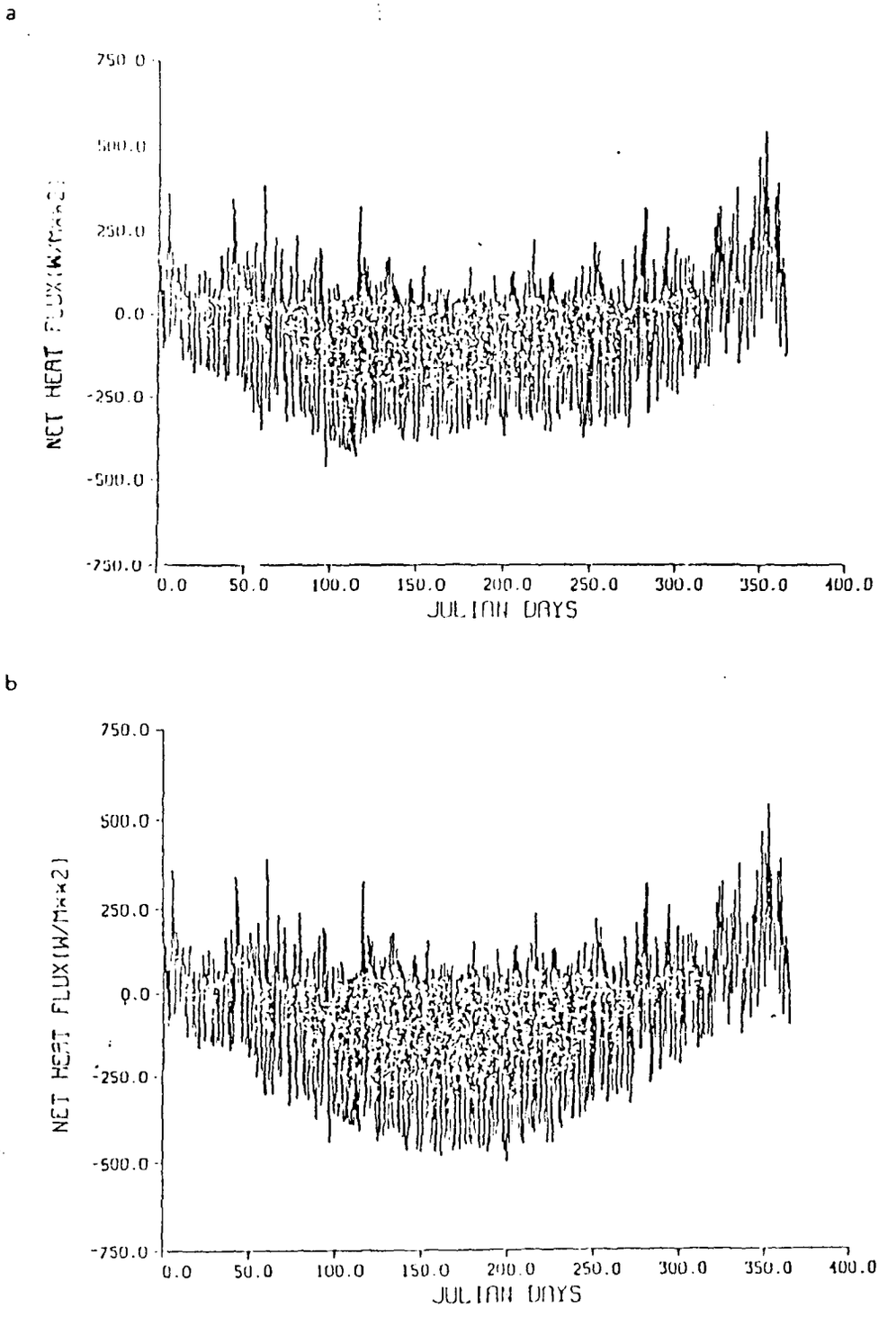

Figure 23. Variation of Net Surface Heat Flux in (a) Complex Event and (b) Simple Event in the Standard Case

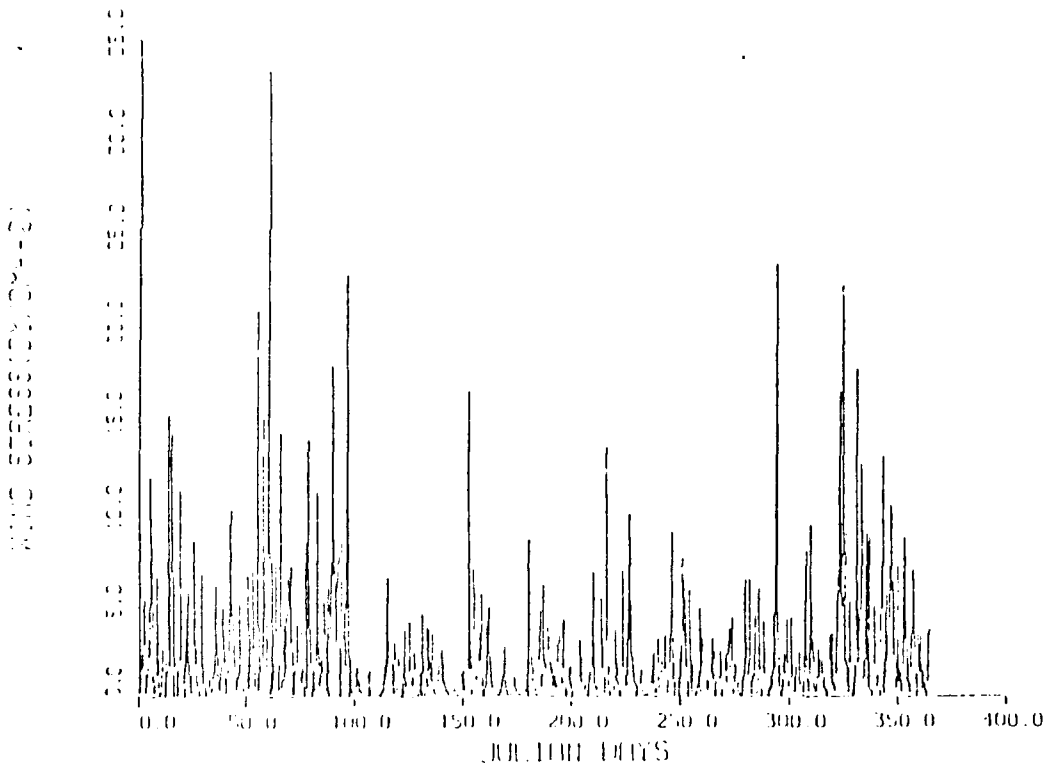

Figure 24. Variation of Wind Stress in 1959

Figure 30). The annual variation of differential MLD and T_s in the variable cloud simulation are shown in Figure 25. An examination of this data will further illustrate some of the difference between the cooling and warming season. Firstly we may note that negative differential MLD frequently appears in the cooling season, while the warming season invariably produces a positive differential MLD. Secondly, the differential T_s decreases from October, the month in which the ocean surface begins to cool, and maintains a constant value, near zero, throughout the winter. In contrast, the differential T_s begins to increase from the spring transition and reaches its maximum value (~7.0°C) in the late summer. Taken together, these two

trends suggest that the albedo effect dominates the mixed layer dynamics during the warming season while the greenhouse effect plays an important role on mixed layer variation during the cooling season.

As summer approaches, the MLD retreats in association with an increase in downward buoyancy flux and reduced winds. For the shallower MLD in Case 1, the solar energy is concentrated in the thinner layer and thus produces a greater negative differential T_s.

During the spring transition (i.e. period between day 100 and day 120) the differential MLD is nearly zero. In contrast, the differential T_s abruptly increases. A similar circumstance develops in late spring between day 177 and day 180. The retreat of the MLD to a thin layer at the ocean surface was true for both the standard case and Case 1 during the spring transition. The unusually small MLD will uniformly result in a lesser differential MLD value while the differential T_s will increase. After late summer the MLD began to deepen and a larger differential appeared, while the differential T_s decreased with the deeper MLD.

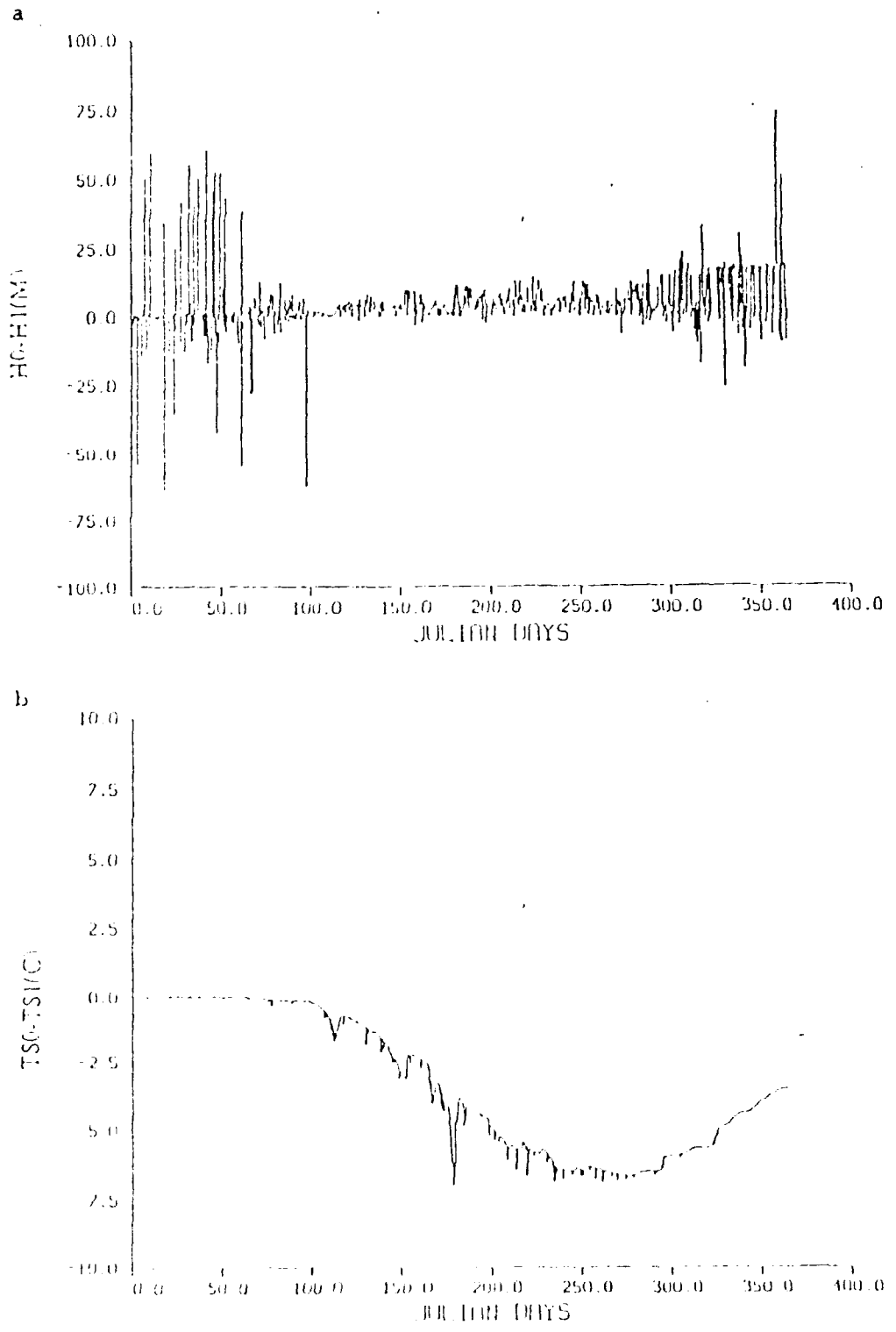

Figure 25. Variation of (a) Differential MLD and (b) Differential T_s in the Variable Cloud Simulation (Complex Event)

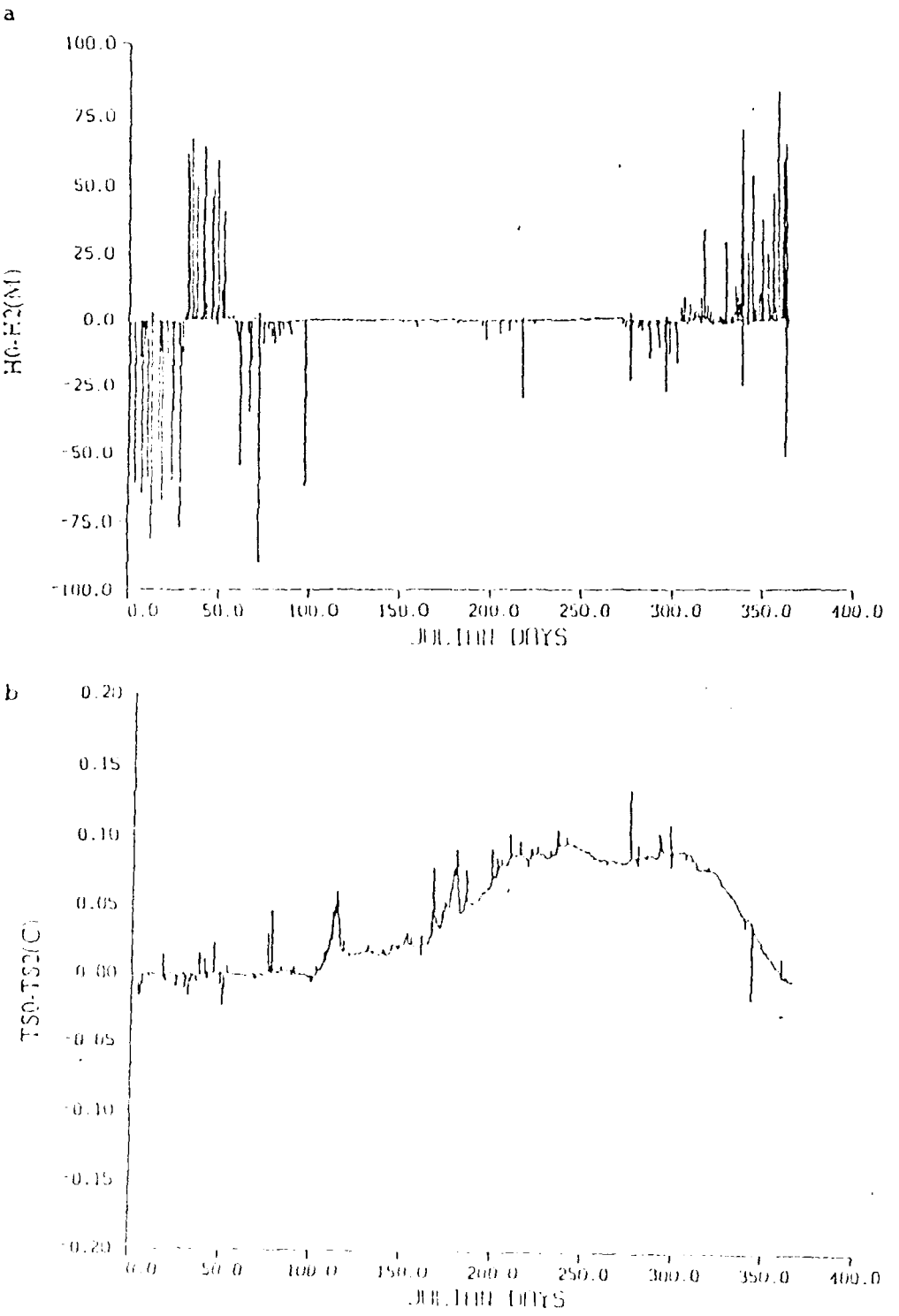

Figure 26. Variation of (a) Differential MLD and (b) Differential T_s in the Variable Precipitation Simulation (Complex Event)

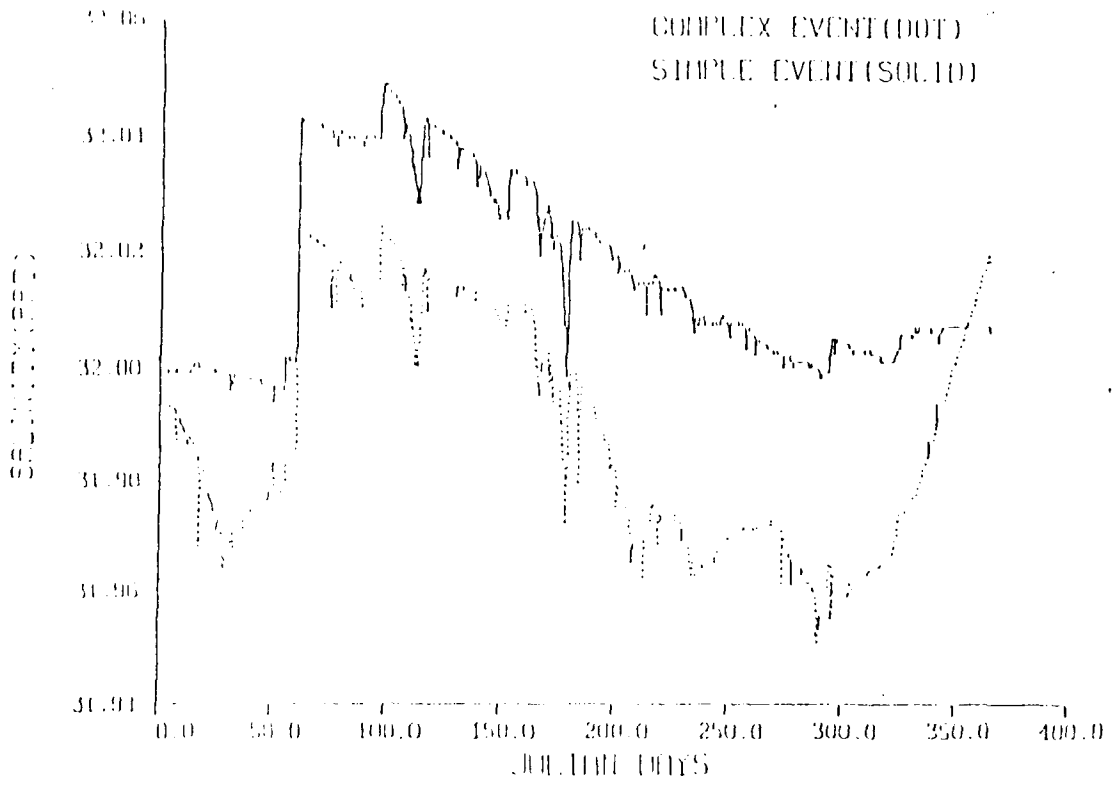

Figure 27. Salinity Variation in Standard Case: The dotted line indicates the complex event; the solid line indicates the simple event

The annual variation of differential MLD and T_s for the variable precipitation experiments is displayed in Figure 26. A positive differential MLD appeared during the cooling season (February, November, and December) when the rate of evaporation was greater than precipitation. The largest negative differential MLD occurs during the months of January, March and October when the precipitation is greatest (see Table 3). The decline of precipitation during the warming season results in a decrease of differential MLD, while precipitation becomes important in its effect on the mixed layer

from late autumn, increasing differential MLD and giving rise to an annual cycle of variation in the differential MLD.

During the winter months, a condition of negative differential T_s prevails as a result of precipitation exceeding evaporation. This induces the MLD in the standard case to be shallower than that found in the case with $E-P_r = 0$, thereby enhancing the rate of cooling associated with winter time net surface heat loss. Note that the magnitude of differential T_s in the variable precipitation experiment is larger than that for the variable cloud experiment during the spring transition. The explanation is related to the fact that solar radiation is still relatively weak in the early spring.

The variation of salinity in Case 2 largely depend upon variation in wind velocity (see dotted line in Figure 27), with large wind increasing the mixed layer salinity in the case with $E-P_r < 0$. This is exemplified by an abrupt increase in mixed layer salinity that occurs at the beginning of March (day 60) when wind velocity is at its strongest for the period (Figure 24). Similar to variations in T_s, mixed layer salinity decreases at a more rapid rate during the spring transition and summer months when wind velocities are low and the MLD is shallow. When late autumn approaches, the mixed layer salinity tends to increase due to erosion of seasonal halocline.

b. Simple Event ($n = 6.7$, $P_r = 62.7$ cm/year, $E_v = 48.7$ cm/year)

Comparing the net heat flux between the complex event and this simple event (Figure 23), we note that during the summer the downward buoyancy flux in the simple event is more pronounced than in the complex event. In the variable cloud simulation the results are similar to those of the

complex event, with the exception of smaller magnitudes of differential MLD and T_s (Figure 28).

The variable precipitation simulation, however, causes a sequence of features quite unlike those found in the complex event (Figure 29). First, the differential MLD has a negative value throughout the entire year, whereas a positive differential MLD occurs in the complex event during the months with an $E-P_r > 0$ configuration. Second, during the late autumn, the decreasing rate of differential T_s is smaller in the simple event. Third, in the simple event, the mixed layer salinity decreases only slightly during the winter and then abruptly increases on day 60 with the arrival of high wind speed. Afterward, mixed layer salinity falls into a pattern of rigid correspondence with the variations of wind velocity, reaching a constant value in late autumn (Figure 27). From Figure 27, we find that the model prediction for the complex event yields at a much closer approximation of the actual salinity profile (i.e. large evaporation in cooling season) than does the prediction for the simple event .

Drawing from BT observations, the actual values of MLD and T_s were compared to those values predicted by the NPS mixed layer model for both the complex and simple events using the standard case category (Figure 30). A distinction exists, in that the BT data shows a deeper MLD profile during the winter months for both simple and complex events and close agreement with the model output for both events during the summer months.

In the general scheme, the values of the model mixed layer temperature compare favorably with observed data. During the winter

months, the BT observations reveal lower temperatures than the model predictions in both complex and simple events. And as we progress through the study period, the actual temperatures increase more than the model predictions for the complex event, which is commensurate with the actual MLD being shallower than the model prediction. During the same time period, circumstances developed wherein a constant cloud cover and precipitation resulted in an extremely shallow MLD, yielding the highest temperatures of summer. With the approach of winter, the actual temperatures are again lower than those of the model prediction for both the complex and the simple events.

A second comparison between the actual recorded data and the model prediction can be made by examining the representations of mean value MLD and T_s in Table 6. The mean observed MLD ($\overline{H}$ = 60.9 m) is almost double that for the complex ($\overline{H}$ = 36.5 m) and simple ($\overline{H}$ = 36.7 m) events, but the mean observed T_s ($\overline{T}_s$ = 8.5°C) is close to the model-predicted value for the complex event ($\overline{T}_s$ = 8.6°C).

TABLE 6. ANNUAL MEAN VALUES OF MLD, TEMPERATURE, NET SURFACE HEAT FLUX AND MIXED LAYER SALINITY

Event	Case	$\overline{H}$ (m)	$\overline{T}_s$°(C)	$\overline{Q}_0$ (w/m²)	$\overline{S}$ (PPT)
Complex	Standard	36.5	8.6	–10.6	31.9
	1	31.9	11.8	–38.4	31.9
	2	36.8	8.5	–10.6	32.0
Simple	Standard	36.7	9.7	–21.4	32.0
	1	31.2	12.5	–43.3	31.9
	2	35.2	9.7	–21.4	32.0
Mean observed MLD = 60.9 m			Mean observed T_s = 8.5°C		

Summarizing the discussion above, we conclude that the model output of MLD for both complex and simple events are in close agreement

with observed MLD in summer. The estimated mixed layer temperature for both events compared favorably with observations, but the estimated mixed layer temperature for the complex event is a little cooler in summer while the estimated mixed layer temperature for simple event is higher in the same period. The mean observed mixed layer temperature is very close to that for the complex event. The model results suggest that observed data is best simulated by model predicting of the complex event.

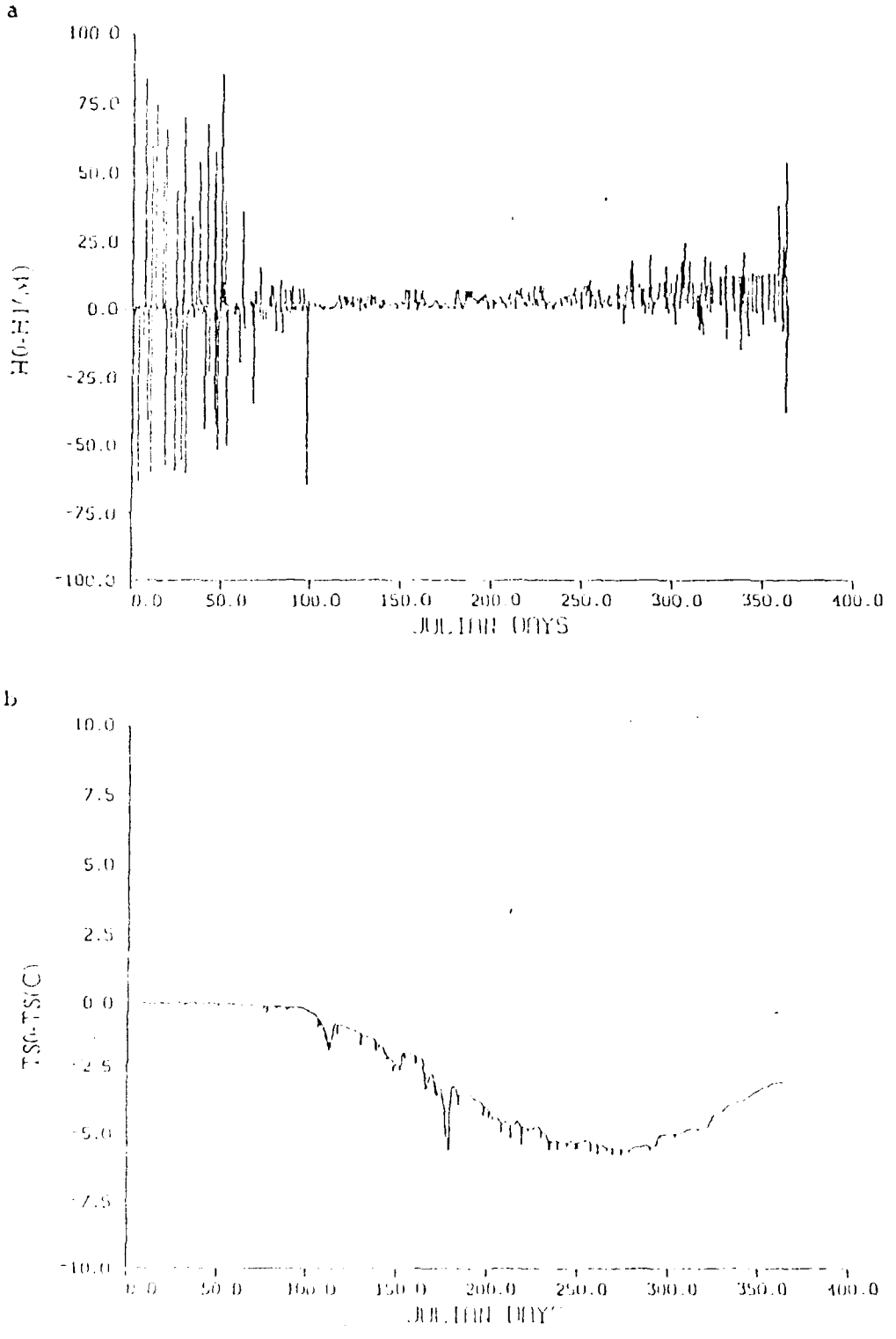

Figure 28. Variation of (a) Differential MLD and (b) Differential T_s in the Variable Cloud Simulation (Simple Event)

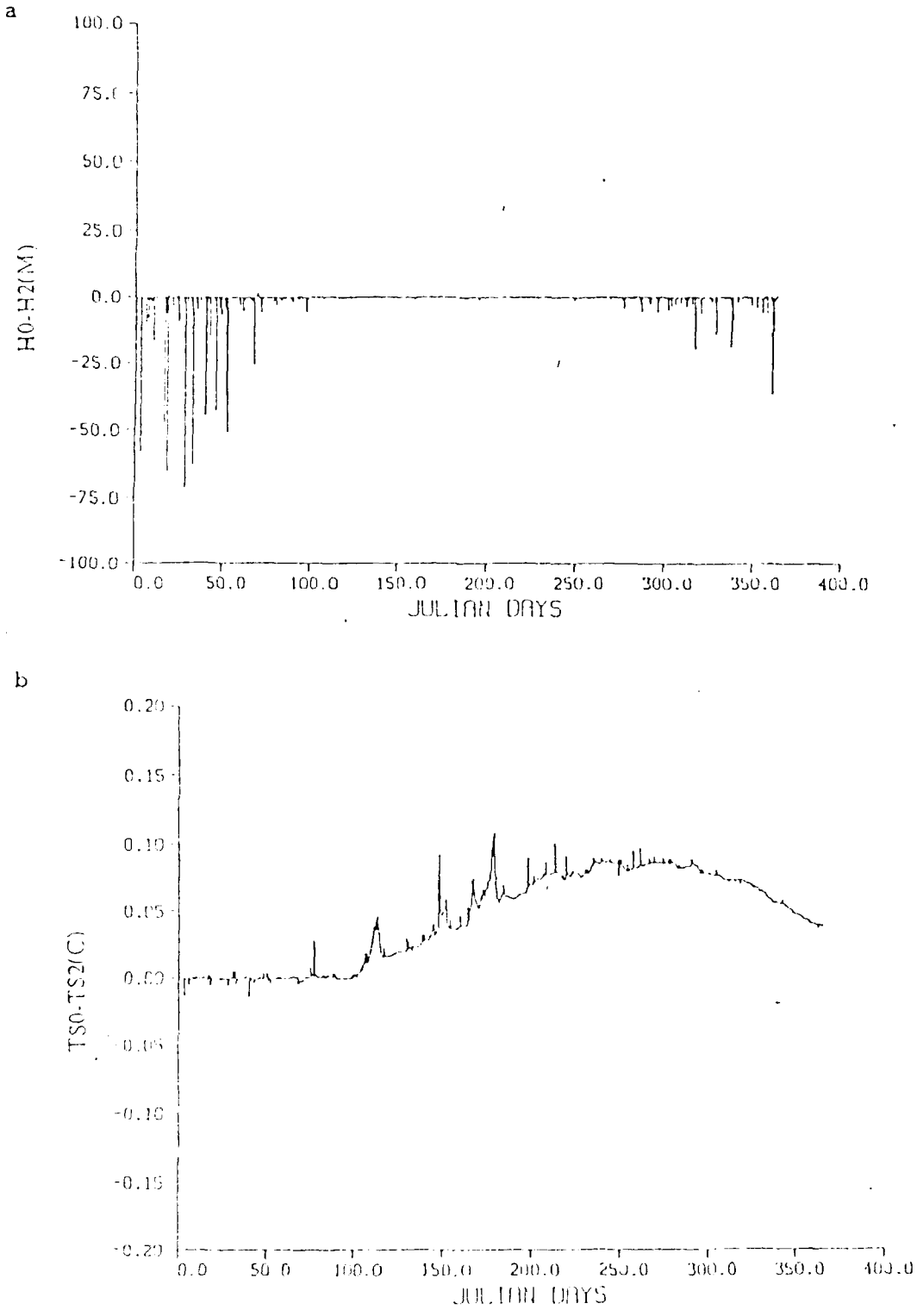

Figure 29. Variation of (a) Differential MLD and (b) Differential T_s in the Variable Precipitation Simulation in Simple Event

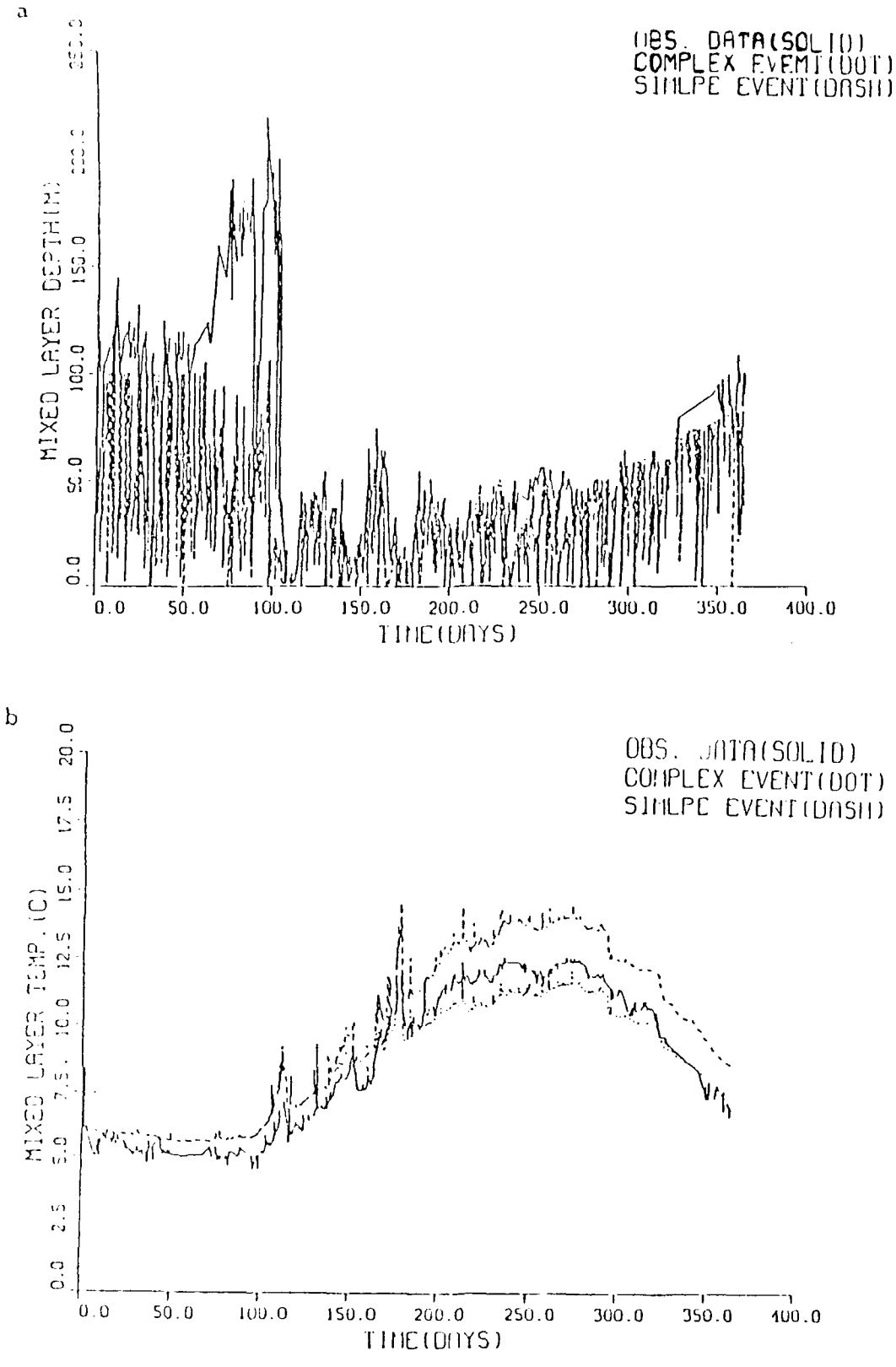

Figure 30. Variation of (a) Mixed Layer Depth and (b) Mixed Layer Temperature in Annual Period: A solid line indicates the observed data, a dotted line indicates the output of standard case in complex event, a dashed line indicates the output of standard case in Simple Event

VI. SUMMARY

This study was conducted to examine the cloud effect on the short-term and seasonal evolution of ocean mixed layer depth, temperature and salinity structure at mid latitudes. The data for this study was collected at Ocean Station Papa located in the Northeast Pacific ocean during 1959. Three kinds of experiments in association with different time scales are designed for this study. Each experiment consists of three cases. The Case 1 simulates a cloud forcing with a 20% reduction of cloud cover from observed data. The Case 2 simulates a simple precipitation forcing with $E-P_r=0$. These two cases are compared with a standard case for which the model cloud are taken as observed .

Three different time scales are selected for this study, that is, 3-day period, 30-day and 365-day periods. For a 3-day period, we examine the albedo and greenhouse effects of cloud and the effect of short-period precipitation events on the ocean mixed layer. Simulations using different amounts of cloud cover indicate that the sensitivity of cloud effect on upper ocean dynamics depends on the direction of the surface buoyancy flux and the length of the day. In winter, the upward buoyancy flux is stronger and the length of the day is shorter, so the greenhouse effect becomes significant on the ocean mixed layer. In contrast, the downward buoyancy flux is stronger and the length of the day is longer during the summer. Thus the albedo effect become significant for ocean mixed layer dynamics. For simulation using different amounts of precipitation, however, we find that the ocean mixed layer is more sensitive to precipitation in winter when wind stirring is predominant.

Similar results are found for a month-long simulation. One striking feature in this period is that both cloud or precipitation have more significant effects on mixed layer temperature and salinity when the mixed layer is very shallow.

For long-term "complex" cloud and precipitation simulations, monthly mean value of cloud cover and precipitation from meteorological observations is derived and tuned to yield realistic cloud coverage and precipitation input for the model. With respect to seasonal variation of solar radiation, the albedo effect is significant during the warming season when the solar radiation is strongest. During the cooling season, the longwave radiation is significant. Therefore, the greenhouse effect plays an important role on upper ocean dynamics. The precipitation effect on the ocean mixed layer is more sensitive during the cooling season due to larger evaporation in winter and smaller precipitation in summer. The resulting values of MLD, temperature and salinity for this complex event are compared with output values for which the model is forced by "simple" constant yearly mean value of cloud cover and precipitation. In general, the model output of MLD in the simple event is shallower than that in the complex event. The mixed layer temperature in the simple event also are higher than in the complex event during the warming season. As for salinity predictions, it shows that the monthly mean values of observed precipitation and calculated evaporation (i.e. complex event) are better used as initial condition for the model.

Finally, the model-predicted values under complex and simple events are compared to observed BT's values. The mean observed MLD($\overline{H}$ = 60.9 m) is much greater than model-predicted values for both complex($\overline{H}$ = 36.5 m)

and simple events($\overline{H}$ = 36.7 m). The mean values of T_s indicates that the mean observed T_s ($\overline{T}_s$ = 8.5°C) is close approximated by the model-predicted values for the complex event($\overline{T}_s$ = 8.6°C). It appears that the observed MLD is in close agreement with that predicted by the model in summer , with the greatest difference occurring in winter. As with MLD, the temperature of complex and simple events generally approximate the temperature cycle and form of the actual data. The temperature in summer provides the greatest difference in comparison with observations in the experiment. The mean values of temperature show that model prediction is close to the actual temperature by using monthly mean value of observations.

There are two reasons why observed MLD and temperature may not agree with model predicted value:

1. The inaccuracies in the BT's data (ship not at fixed location & real ocean not one-dimensional).
2. The inaccuracies in model forcing, especially in producing surface buoyancy flux in variable cloud simulation.

The cloud model scheme case in this study is very crude, therefore inaccuracies in calculating buoyancy flux for the model in variable cloud experiment may exist. As mentioned before, the cloud is the most significant factor which influences the sea surface temperature due to the reduction in solar radiation or emission of longwave radiation back to the ocean surface. The decreasing or increasing sea surface temperature may diminish or produce more clouds. This feedback mechanism may couple the cloud-ocean mixed layer system. In this study, we are only concerned with the mechanism of clouds on the ocean mixed layer, therefore the resulting

analysis might be biased by lack of information of this feedback mechanism in the cloud-ocean mixed layer system.

It is recommended that this model experiment should be expanded by coupling with an atmospheric boundary layer model that includes feedback mechanisms between atmosphere and ocean. Furthermore, the precipitation induced from satellite imagery can be used as input to the NPS mixed layer model for getting a more accurate solution. Finally, this experiment may help to focus attention on the importance of cloud variability on ocean mixed layer because it has been shown here to be the most complex and least understood aspect of upper ocean dynamics.

LIST OF REFERENCES

Budyko, M. I., 1978: The heat balance of the earth, Cambridge Univ. Press, pp. 85-113.

Chu, P. C. and R. W. Garwood, 1989: Thermodynamic feedback between clouds and the ocean surface mixed layer, *Advances in Atmospheric Sci.*, **7**, pp. 1-10.

Chu, P. C. and R. W. Garwood, 1989: Unstable and damped modes in coupled ocean mixed layer and cloud models, *Jour al of Marine Systems*, **1**, pp. 1-11.

Denman, K. L. 1973: A time-dependent model of the upper ocean, *J. Phys. Oceanogr.*, **3**, pp. 173-18.

Denman, K. L. and M. Miyake, 1973: Upper layer modification at Ocean Station "Papa" observation and simulation, *J. Phys. Oceanogr.*, **3**, pp. 185-196.

Elsberry, R. L., T. S. Fraim, and R. N. Trapnell, 1976: A mixed layer model of the oceanic thermal response to hurricanes, *J. Geophys. Res.* , **81**, pp. 1153-1162.

Garwood, R. W., 1977: An Ocean Mixed Layer Model Capable of Simulating Cyclic States, *J. Phys. Oceanogr.*, **7**, pp. 455-468.

Garwood, R. W., 1977: Air-sea interaction and dynamics of the surface mixed layer, *Rev. Geophys. Space Phys.*, **17**, pp. 1507-1524.

Garwood, R. W. and D. Adamec, 1982: Model simulations of seventeen years of mixed layer evolution at Ocean Station Papa, Research project of departments of oceanography and meteorology, Naval Postgraduate School, Monterey, CA. 37 pp.

Geisler, J. E. and E. B. Kraus, 1969: A comparison of seasonal thermocline models with observation, *Deep Sea Res.*, **23**, pp. 391-401.

Husby, D. M., and G. R. Seckel, 1978: Large-scale air-sea interaction at Ocean Station "V", *NOAA Tech. Rep. NMFS SSRF-696*, 44 pp.

Kraus, F. B., and J. S. Turner, 1967: A one-dimensional seasonal model of seasonal thermocline. II. General Theory and its Consequences, *Tellus*, **19**, pp. 98-106.

Kim, J., 1976: A generalized bulk model of the oceanic mixed layer, *J. Phys. Oceanogr.*, **6**, pp.686-695.

Livezey, M. S., 1988: Discrete precipitation effects on the seasonal mixed layer dynamics in the North Pacific Ocean, Master's Thesis, Naval Postgraduate School, Monterey, California, 71 pp.

Laevastu, T., 1960: Factors affecting the temperature of surface layer of the ocean, *Soc. scient. Femica. Comment. Physico.-Math.*, **25(1)**, pp.1-136.

Miller, J. R., 1976: The salinity effect in a ocean mixed layer model, *J. Phys. Oceanogr.*, **6**, pp. 29-35.

Miropol'skiy, Yn. A., 1970: Nonstationary model of the wind-covection mixing layer in the ocean, *Izv. Atmos. Oceanic Phys.*, **6**, pp. 1284-1294.

Seckel, G. R. and F. H. Beaudry, 1973: The radiation from sun and sky over the North Pacific Ocean, *EOS, Trans. Am. Geophys. Union*, **54**, pp.1114.

Tabata, S., 1961: Temporal changes of the salinity, temperature and dissolved oxygen content of the water at Station Papa in the Northeast Pacific Ocean, *J. Fish. Res. Bd. Can.*, **18** , pp. 1073-1124.

Tabata, S., 1965: Variability of oceanographic condition at Ocean Station Papa in the Northeast Pacific Ocean, *J. Fish. Res. Bd. Can., III Series IV*, pp. 367-418.

Tabata, S., 1964: A study of the main physical factors governing the oceanographic conditions of Station Papa in the Northeast Pacific Ocean, Ph.D. Thesis, University of Tokyo, 264pp.

Thomson, R. E., 1971: Theoretical studies of the circulation of the subarctic Pacific region and the generation of Kelvin tvpe waves by atmospheric disturbance. Ph. D. Thesis, Institude of Oceanography, University of British Columbia.

INITIAL DISTRIBUTION LIST

1. Defense Technical Information Center 2
   Cameron Station
   Alexandria, VA 22304-6145

2. Library, Code 0142 2
   Naval Postgraduate School
   Monterey, CA 93943-5002

3. LCDR Wu Pao-Kun 6
   94. Sec. 2, Kung Yen Rd.
   Changhun, Taiwan R.O.C.

4. Library 1
   Chinese Naval Academy
   Kaoshiung, Taiwan R.O.C.

5. Department of Oceanography
   Naval Postgraduate School
   Monterey, CA 93943-5000
   Attn: Chairman, (Code OC/Co) 1
   Attn: Dr. R. W. Garwood (Code OC/Gd) 1
   Attn: Dr. P. C. Chu (Code OC/Cu) 1

6. Department of Meteorology
   Naval Postgraduate School
   Monterey, CA 93943-5000
   Attn: Chairman, (Code MR/Rd) 1
   Attn: LCDR T. C. Yin (SMC 2408) 1

7. Commanding Officer 1
   Navy Headquarters
   Taipei, Taiwan, R.O.C.

8. Commanding Officer 1
   Naval Hydrographic & Oceanographic Office
   Tso-Ying, Kaoshinng, Taiwan, R.O.C.

9. Commanding Officer 1
Naval Oceanographic Officer
NSTL Station
Bay St. Louis, MS 39522

10. Commander Officer 1
Fleet Numerical Oceanography Center
Monterey, CA 93943

11. Commanding Officer 1
Naval Ocean Research and Development Activity
NSTL Station
Bay St. Louis, MS 39522

12. Office of Naval Research (Code 1120PO) 1
800 N. Quincy St.
Arlington, VA 22217

13. Commanding Officer 1
NOARL-W
Monterey, CA 93943

14. Dr. Susuma Tabata 1
Institude of Ocean Sciences
Box 6000
9860 West Saanich Road, Sidney, British Columbia
Canada, V8L 4B2

15. Dr. Peter Muller 1
Department of Oceanography
University of Hawaii, Honolulu, HI 96822